KIT SCIENTIFIC REPORTS 7637

Design Strategy for the PFC in DEMO Reactor

Yu. Igitkhanov, B. Bazylev, I. Landman and R. Fetzer

KIT Scientific Publishing

Yu. Igitkhanov, B. Bazylev, I. Landman and R. Fetzer

Design Strategy for the PFC in DEMO Reactor

Karlsruhe Institute of Technology
KIT SCIENTIFIC REPORTS 7637

Design Strategy for the PFC in DEMO Reactor

by
Yu. Igitkhanov
B. Bazylev
I. Landman
R. Fetzer

KIT Scientific Publishing

Report-Nr. KIT-SR 7637

Impressum

Karlsruher Institut für Technologie (KIT)
KIT Scientific Publishing
Straße am Forum 2
D-76131 Karlsruhe
www.ksp.kit.edu

KIT – Universität des Landes Baden-Württemberg und
nationales Forschungszentrum in der Helmholtz-Gemeinschaft

KIT Scientific Publishing 2013
Print on Demand

ISSN 1869-9669

Table of content

I. Introduction

The performance of the plasma facing components (PFC) and materials in fusion reactor DEMO are fundamental issues affecting the ultimate technological and economic feasibility of fusion power. Many factors influence the choice of a functional and structural material in a fusion reactor. Component lifetime is mainly limited by radiation damage, disruptions, and sputtering erosion. Our design strategy is to determine the structure and coating thicknesses, which maximize component lifetime against all life limitations. At present, the stainless steel modifications (EUROFER) remain the primary choice for a structural material because of the large existing database and industrial capability. Tungsten alloys are the primary materials for the plasma-facing surface in DEMO. Although W/EUROFER bound is compatible with high neutron fluencies to minimize the necessary replacement of the in-vessel components and is "low-activation" type, the loss of creep strength at relatively low temperatures could be the main drawback of EUROFER as a structural material in the case of low or moderate wall temperatures. That is why the realization of the FW sandwich-type blanket with W as an armour material and EUROFER as a structural material must be investigated as a most promising combination. Moreover, the reinforcement by SiC fibers or oxide dispersion strengthened (ODS) steels may potentially improve the high temperature creep resistance of EUROFER steel.

It is shown that apart from the fact that W/EUROFER bound is compatible with high neutron fluencies and is "low-activation" type (thus minimizing the necessary replacement of the in-vessel components), EUROFER steel as a structural material will remain creep resistant in the case of the 'hot wall' operation. However, high temperature wall causes a fundamentally different physical chemistry regime for wall surface erosion.

After calculation of erosion and thermal material destruction due to plasma impact by means of MEMOS and ENDEP codes (B. Bazylev et.al, J. Nucl. Mat. 307-311, 69 2002), we present the lifetime analysis for W and EUROFER materials under DEMO operation conditions. Finally, we consider the efficiency of helium and supercritical water as a coolant and compare their advantages and disadvantages for high temperature DEMO operation.

We analyze a sandwich-type blanket configuration of W/EUROFER for DEMO first wall under steady-state normal operation and off-normal conditions, such as vertical displacements and runaway electrons. The heat deposition and consequent erosion of the tungsten armor is modeled under condition of helium cooling of the first wall blanket module and by taking into account the conversion of the magnetic energy stored in the runaway electron current into heat through the ohmic dissipation of the return current induced in the metallic armor structure. It is shown that under steady-state DEMO operation the first wall sandwich type module will tolerate heat loads up to~14MW/m^2. It will also sustain the off-normal events, apart from the hot vertical displacement events, which will melt the tungsten armor surface.

The life-time performance is analyzed in details for the steady-state operation when sputtering erosion playes dominant role. The sputtering erosion of the first wall tungsten armor layer due to the plasma impact is evaluated. It is shown that for DEMO conditions the total sputtering erosion of W armor by the charge-exchange DT neutrals could at least reach~1mm during one year of steady-state operation.

The off-normal and transient events could pose a severe tread causing a melt-erosion and thermal fatigue in functional and structural materials in fusion reactor DEMO. We analyze the impact of unmitigated edge localized modes (ELMs) on the first wall sandwich type blanket module. The expected ELMs characteristics for DEMO are estimated by extrapolating predictions made for ITER and by using the scaling arguments. The tungsten and EUROFER material damage and effect of melt layer motion on the subsequent ELM loads is numerically investigated by using the MEMOS code. It is shown that due to the ELMs repetition impact the total tungsten surface roughness will considerable grow. The magnitude of roughness after many ELMs with the heat loads stochastically distributed over the divertor surface. It is proven that the considerable

alleviation of ELMs in DEMO will ultimately require. The effect of runaways and vertical displacement events is also considered under DEMO conditions.

The main results discussed in this preprint have been reported in the following conferences: in PSI 2012Aachen 21– 25 May 2012, in ANS 20th Topical Meeting on the Technology of Fusion Energy (TOFE-2012) Nashville 27-31 August and in the 27th Symposium on Fusion Technology (SOFT) Liege 24-28 September 2012. The corresponding papers submitted to Journal of Nuclear Materials and Fusion Engineering and Design. Some papersa are alrsdy published, the other will be published in special issues during 2013. Some results were also reported on the 17th Joint EU-US Transport Task Force Meeting, Padova (September 3-6, 2012), on the 20th European Fusion Physics Workshop, Ericeira, Portugal (3-5 December 2012) and during the DEMO related meetings in Culham and in Garching.

After general introduction in chapter I, we begin in chapter II with the discusson of the applicability of Tungsten/EUROFER Blanket Module for the DEMO FW in the case of off-normal operation conditions. Then in chapter III we will discusse some problems related to the DEMO steady-state operation, namely: the plasma impact on the first wall (FW) during a long period of operation and the plasma–wall interaction associated with sputtering erosion during a long pulse exposition of heat and particle flux into the FW tungsten armor and consequent bulk plasma contamination. In chapter IV effect of reperitive edge localized mode (ELMs) on reactor first wall is discussed. Finaly, we present some conclusive remarks. In attachents, we present some reference data and the results that are still under preparation for publications. It concerns to analysis of a singl-noul x-point configuration with respect to coupling of ballooning instability with thermal (MARFE) instability under DEMO conditions and the role of perpendicular energy transport on the impurity radiation in the SOL and divertor region. Both these issues are subject of EFDA DEMO tasks for 2012-2013.

II. Applicability of Tungsten/EUROFER Blanket Module for the DEMO FW

Yu. Igitkhanov, B. Bazylev, I. Landman and L. Boccaccini, presented in 20th PSI Conference, Aachen, Germany, 21. - 25.05.2012;
Y.Igitkhanov et al., J.Nucl. Mater.(2013), http://dx.doi.org/10.1016/j.jnucmat.2013.01.089

In this paper we analyse a sandwich-type blanket configuration of W/EUROFER for DEMO first wall under steady-state normal operation and off-normal conditions, such as vertical displacements and runaway electrons. The heat deposition and consequent erosion of the tungsten armour is modelled under condition of helium cooling of the first wall blanket module and by taking into account the conversion of the magnetic energy stored in the runaway electron current into heat through the ohmic dissipation of the return current induced in the metallic armour structure. It is shown that under steady-state DEMO operation the first wall sandwich type module will tolerate heat loads up to~14MW/m^2. It will also sustain the off-normal events, apart from the hot vertical displacemet events, which will melt the tungsten armour surface.

1. Introduction

A sandwich type first wall (FW) blanket module made of W-clad EUROFER steel (see Fig. 1) is examined against the normal and off-normal operation heat loads expected in DEMO reactor. The module consists of a helium coolant tube of rectangular cross-section within the EUROFER matrix that is used as heat diffuser. The plasma material interface in DEMO is more challenging than in ITER, due to the requirements for approximately four times higher heat flux from the plasma and approximately five times higher average duty factor [1]. We consider here the DEMO design of ~1GW of electric power, the major redius R=7.7m, the aspect ratio A=3, the toroidal magnetic field B=6T and the safity factor q_a=4.5 [2]. The heat load to the FW under normal steady-state operation is expected to be in the range of 0.5-15 MW/m^2 and a considerable amount of energy (>90%) is radiate by light impurities injected into plasma boundary [3, 4]. Heat loads above 0.5MW/m^2 could mainly be expected due to interaction with hot charge-exchange neutral atoms and due to convective radial plasma losses, associated with unstable convective cells in the SOL region. To achieve sufficient cooling efficiency under such an excessive heating helium gas as a coolant must be employed, which has no limitation on heat flux value like water, considered previously [4].

Below we consider two types of off-normal events: a loss-of control “hot” and following a disruption “cold” vertical displacemen events (VDE) and runaway (RE) generation that can occur during the current quench following a disruption. Both, VDE and RE energy deposition would affect mostly the first wall [5]. The consequent erosion due to excessive power and particle loads on plasma facing components (PFC) is expected in DEMO, particularly, because of a huge amount of poloidal magnetic energy (~1.2GJ) which will eventually dissipate in the material structure. We evaluate here the conversion of magnetic energy into heat due to mainly ohmic dissipation of return current, induced during the penetration of RE beam into the tungsten armour.

Although W/EUROFER bound is of “low-activation” type, it has relatively low creep temperature (823°K) which could be the main drawback of EUROFER as a structural material. To assess proper design parameters of the FW module, calculations were performed with the Monte Carlo Energy Deposition code ENDEP together with the upgrated version of MEMOS code [6], which takes into account helium as a coolant and the RE magnetic field energy convertion into heat. The details of the RE modelling by means of ENDEP code are described in [3,4]

2. Energy loads on the FW DEMO during off-normal events

The characteristics of off-normal events in DEMO one can assesse based on scaling arguments by extrapolating data envisaged for ITER [1, 3, and 4]. In the case of VDE which may occur due to accidental loss of control in DEMO, we assume that ≤ 2GJ (~0.7GJ of plasma thermal energy and ~1.2 GJ of magnetic energy) will eventually deposit on the FW structure. The resulting energy density can be estimated in the range of ~50-100 MJ/m^2, which includes toroidal and poloidal peaking factors similar to ITER and assumption that the deposited area~$2\pi Rd$ is about 25-50m^2 corresponding to toroidally continuous band d = 0.5-1m and the DEMO major radius R=7.5m. In this case of accidental control loss the plasma column drifts toward the wall with the resistive growth time of vessel structure, which we assume in DEMO similar to ITER - of the order of ~0.5-1sec. In the case of 'cold' VDE, when vertical instability arises after thermal quench, current channel moves towards the wall during current decay and deposits remaining energy to the FW (similar to JET [5]). We take in our calculations the worst case assumption that the magnetic energy deposits to the FW surface band of 25m^2 over~0.5-1 sec. Since the stored plasma energy in DEMO is by at least a factor of two higher than that in ITER [1], the kinetic energy of REs in DEMO can be assumed as W_{kin}~20MJ x 2≈40 MJ [3]. Slow RE loss is accompanied by transformation of magnetic energy in RE kinetic energy. Fast RE losses triggered by major MHD modes will occur on the Alfven time scale of τ_{MHD}~R/c_A~15μs, where R=7.5m is plasma major radius and c_A~6.10^5 m/s is Alfven velocity for poloidal field B_p~0.4T [2]. During this short time the plasma column can be considered stationary as whole. RE velocity normal to the FW surface will be determined by plasma convection on MHD time scale V_{perp}~a/τ_{MHD}~2 10^5 m/s, where a=2.5m is the minor radius. Thus, the incident angle (on axisymmetric wall) is V_{perp}/c ~10^{-3} and RE SOL thickness is Δ_{SOL}~$2\pi qRV_{perp}/c$~0.27 m, q~3 is the safity factor. One can assume that during the fast loss magnetic energy is not transferred to RE kinetic energy and the total energy of RE is 40 MJ [3]. The poloidal length of RE wetted area is about H~$(2a\Delta_{SOL})^{1/2}$~1m [7]. It is likely that plasma will be toroidally asymmetric during this event with large n=1 perturbation of its shape and thus the worst case assumption is that all RE will be deposited on a single or a few toroidal FW section. If deposition occurs on 1/3 of the toroidal circumference, then the wetted area can be estimated as ~$1/3\cdot(2\pi R)\ (2a\Delta_{SOL})^{1/2}$≈16m^2. Therefore, the RE kinetic energy density of ~50-70MJ/m^2 is expected in DEMO FW. We assume that the total RE energy varies in the range of 30-100 MJ/m^2, keeping in mind that part of the poloidal magnetic energy could eventually also be converted into RE kinetic energy [5] and (like in JET) a large fraction~40% could dissipate in the plasma-coupled conducters. The RE current can be estimated as I_{re} ~10-15MA, which is about ≤70% of the total plasma current (similar to estimations for ITER). In our calculations we also assume that the energy deposition time of RE is in a range of 0.05-1s. This roughly corresponds to the loss time of high-energy REs due to the fact that their drift orbits intersect the wall in resistive time scale and this time depends on the thickness of the wall structure. Specifications of energy loads on DEMO FW are summarized in TableI.

3. Conversion of the RE magnetic energy into heat

The particular interest occurs when RE impinging on the FW and depositing their kinetic and magnetic energy into tungsten armor. The correct evaluation of deposited energy is important for assessment of surface erosion and plasma contamination. Usually, the evaluation of stopping power takes into account only the kinetic energy of impinging electrons. Here we consider the mechanism of inductive losses of the RE beam in tungsten armour. When an RE beam intersects a tungsten surface, the beam space charge within a metal is effectively neutralized by a redistribution of the free electrons of the metal with the characteristic time $\tau \sim 1/\omega_p$~10^{-16} sec, where the plasma frequency of tungsten ω_p is~9.74 10^{15} sec^{-1} and the effective electron mass $m_{e,eff}$ ~2-3m_e. This time is typically quite short, so that net space charge does not limit the RE penetration in a metal. The

RE current I_{RE} will induce a return ohmic current I of free electrons in tungsten, which acts to neutralize the magnetic field of the RE, so that $I_{RE} \sim -I$ during short time and if $\lambda_E/a << 1$ (where a is the RE beam radius, $\lambda_E \sim c/\omega_p \sim 3\mu m$ is the electron skin length). The ohmic dissipation of plasma current and a drag between the RE beam and the induced electric field eventually converts the RE magnetic energy into heat. The ratio of the magnetic energy converted into heat can be evaluated by solving the equation, describing the evolution of induced electric field E. The energy balance of plasma heated by a return current driven by a relativistic electron beam can be given as:

$$\frac{d}{dt}W_{mag} = -RI^2 - 2\pi RcE \cdot I_{RE}, \quad (1)$$

where R is the resistance of the metal per unit length, W_{mag} is the magnetic energy of the RE beam and the last term corresponds to energy loss due to the work done by the RE beam [8]. Calculations of collisional damping of the induced current are presented in Fig. 2, where the RE magnetic energy loss in W armour is plotted against the deposition time for the different W armour temperatures. It is seen, that for expected deposition time in DEMO (t ~ 0.3-0.5sec) substantial portion of poloidal magnetic energy ≤ 1GW will be dissipated in tungsten for surface temperatures ≥1500K. The dissipation increases for higher temperatures because of the resistivity increase. These assessments are included in the MEMOS evaluation of the energy deposition of RE beams inside the W metallic armour.

4. Helium active cooling of the FW module

Here we analyse the helium coolant capability of the heat removal for the FW blanket module under DEMO conditions based on a model of turbulent flow in rectangular channel. In our model the helium coolant flows through a rectangular channel with square cross-section ~15mm×15mm. The channel passes through the EUROFER and positioned with wall thickness of 3.5 mm on the plasma facing side and 11.5mm on the side facing the breeding units (Fig. 1). To stay within the allowed temperature window for the EUROFER steel, a high heat transfer is required. In previous work [4] we found that water coolant restricts operation below some critical heat fluxes. Helium gas coolant has no such restrictions and is applicable for very high coolant temperatures. Following [9], we apply the model for a single-phase water flow for helium coolant. The heat flux q_w removed by coolant, can be estimated as $q_w = h \cdot f \cdot (T_w - T_c)$. Here h is the heat transfer coefficient, were T_w is the wall temperature average over channel length, T_c is the coolant temperature average over channel length, and and the convective heat transfer coefficient h=Nu·χ/D estimated for turbulent helium flow according to the simple Dittus–Boelter correlation $Nu=0.023Re^{0.8}Pr^{0.4}$. Here Nu is the Nusselt number for turbulent flow of helium, Re is the Reynolds number, Pr is the Prandtl number and χ is the helium thermal conductivity. A factor f accounts for 2D effects due to one-sided heat flux to the coolant ($f \sim \Delta/0.5\pi D$, where Δ is the pitch, D is the equivalent tube diameter) [9]. The boundary condition for thermal diffusion equation at the tube wall is based on equating the conduction heat flux at the wall to the convective heat flux to the coolant:

$$-\chi \cdot \left(\frac{\partial T}{\partial x}\right)_w = h \cdot f \cdot (T_w - T_c) \quad (2)$$

The Helium temperature in outlet, T_c, is calculated from the inlet gas temperature, T_{c0}, helium mass velocity u and heat flux over a tube length q_w: $T_c = T_{c0} + f \cdot q_w / \rho u c_p$ where ρ is the mass density of

Helium and c_p is its specific heat. The pressure drop along channel depends on the coolant mass velocity, the density, the friction factor, μ [9], the coolant channel hydraulic diameter, D'

$$\left(\frac{\partial p}{\partial x}\right) = -\mu \frac{\rho u^2}{2D'}\left(T_w - T_c\right) \quad (3)$$

and can be estimated by integrating over the channel length. This model incorporated into the MEMOS code for evaluation of heat flux transfer through the entire module to a coolant. The data pertaining to Helium where taken from [10]. The Reynolds and Prandtl numbers evaluated at the mean flow temperature are Re $\geq 2\text{-}5 \cdot 10^5$ and Pr ≥ 0.67, thus confirming the applicability of the turbulent model under DEMO conditions The required heat transport coefficient is ~ 6 kW/m^2/K and the resulting high fluid velocities are in the range of 60-190m/s depending on the removal heat flux. Under these conditions, EUROFER stays below the allowed temperature $\leq$550ºC. Fig. 3 shows the power removed by helium flow and corresponding values of the averaged tube and the He temperatures. The required coolant flow velocities and pressures at inlet have also indicated in the same plot. Calculations show that helium coolant allows one to remove thermal power under expected in DEMO steady-state heat loads keeping the material temperatures below the EUROFER creep point and W armour below the melting point (3410 ºC). The advantage of helium coolant is its compatibility with higher temperature. The disadvantage of helium coolant as a gas is the relatively low heat transfer coefficient that can be achieved by conventional pipe cooling. To have higher heat transfer coefficient required for cooling FW blanket module ($h \geq 5$ kW/m^{2}K) high flow velocity should be achieved by increasing the pressure drop. Our results indicate that high pressure is needed to compensate the low helium gas pressure and the relative low thermal diffusivity. This could require a big pumping power which necessary to circulate in the system and could reduce the efficiency of the power conversions. Nevertheless, his adaptability to any operational temperature makes helium very suitable for application in DEMO.

5. Numerical results and analysis

Calculation where performed for armour thickness Δ_w = 3mm and for EUROFER thickness $\Delta_{EUROFER}$ = 4mm. and at high helium cooling efficiency (u=150m/s and 190MPa). Fig. 4 shows the surface temperature of the tungsten armour and the maximum EUROFER temperature (interlayer temperature) for different heat loads in steady-state regimes of operation. Both temperatures increase with the increase the heat load. For heat loads above14MW/m^2 the EUROFER temperature exceedes the creep point T_c = 823K and EUROFER looses its creep strength [6]. Calculations show that in the range of heat fluxes 0.5-12MW/m^2 and under helium cooling conditions the W armour thickness Δ_w=3mm is optimal - it does not melt and protects EUROFER from excessive heating. As it is shown in [4] this thickness is sufficient to tolerate about three years of continuous reactor operation by taking into account only the sputtering erosion. Results of calculation for off-normal events are presented in the Fig. 5, 6. In Fig.5 the temperature of W amour surface is shown as a function of armor thickness for different events. Fig.6 shows the maximum of EUROFER temperature depending on W armour thichkness. Calculations show, that in the case of disruption with the hot VDE the energy deposition into the armor will cause strong surface melting up to 0.07mm and evaporation up to a few mm. In the case of cold VDE with or without RE tungsten temperature remains below the melting point. The same found for RE impact. Both slow and fast RE loss will not cause the melting of W armor surface, although the wetted area for RE is smaller. In the case of RE fast losses, they depositing almost all kinetic and about 40% of magnetic energy into armour, the W surface temperature does not exceed~2000 K because of very short deposition time~0.01ms. In the all cases (except for the RE slow loss) the armor temperature is quite independent on armor thickness, because heat deposition takes place in a thin surface layer. In the case of the RE slow loss heat deposition occurs deeper in armor and heating time becomes

comparable with heat diffusion time for W thicknesses ≤ 1cm. This explains the W temperature decrease with increasing the armor thickness. The maximum EUROFER temperature drops with increasing the W armor thickness (see Fig. 6) and does not melt for the all considered cases.

6. Conclusions

1) Under steady-state normal operation and helium cooling the FW W/EUROFER blanket module can tolerate expected in DEMO heat loads without W armour melting and EUROFER thermal destruction. For Δ_W~3mm, $\Delta_{EUROFER}$~4mm the maximum tolerable heat flux is about 14MW/m^2.
2) To achieve efficient heat transfer required for helium cooling of the FW blanket module in DEMO, a high flow velocity (≥ 100m/s) should be achieved by increasing the pressure drop (~ up to 200MPa inlet pressure). This, unfortunately, could require large pumping power.
3) Direct conversion of the RE magnetic energy into heat within a metallic armor occures du to ohmic dissipation of the return current of free electrons and depends on W surface temperature and RE pulse duration.
4) In the case of hot VDE the W armor is not tolerate the heat load: it melts down to 0.07mm and intensively evaporates up to a few mm during 0.5sec.The RE fast loss case does not cause the W armor melting because of a very short exposure time ~0.01ms. For slow losses the RE deposit their energy (magnetic and kinetic) deeper in armor layer, which explains the W temperature decrease with increasing the armor thickness.

Acknowledgments: This work, supported by the European Communities under the contract of Association between EURATOM and Karlsruhe Institute of Technology, EURATOM and CCFE, was carried out within the framework of the European Fusion Development Agreement. The views and opinions expressed herein do not necessarily reflect those of the European Commission**.**

References

[1] ITER Physics Basis, Chapter 9: ITER contributions for Demo plasma development, *Nucl. Fusion* 47, (2007) S404; ITER DDD, WBS1.9, Physics Section 6.3, 1983
[2] D. Maisonnier et al., Nucl.Fusion 47 (2007) 1524
[3] Yu. Igitkhanov, B. Bazylev, Fusion Science and Technology, 60 (1) (2011), 349.
[4] Yu. Igitkhanov, B. Bazylev, Fusion Eng. Des. (2012), doi:10.1016/j.fusengdes.2012.01.013
[5] A. Loarte, V. Riccardo et al., *Preprint EFDA–JET–PR(10)*, **23**, 2010
[6] Yu. Igitkhanov, B. Bazylev and I. Landman, *J. Nucl. Mat*. (2010) 415, S845
[7] S. Putvinski, ITER, private communication
[8] L.Thode and R.Sudan The Physics of Fluids, Vol. 18, No. 11, November 1975
[9] G. Federici, A.R.Raffray, Journal of Nuclear Materials 244 (1997) 101
[10] H. Petersen, *The Properties of Helium*, Danish Atomic Energy Commission, Report No. 224, 1970

Figure Captions

Fig. 1 Mock-up of a sandwich type W/EUROFER blanket first wall module used for the Monte Carlo MEMOS computation of the plasma impact.
Fig. 2 Conversion of the RE magnetic energy into heat in W armour vs RE exposure time for different W temperatures and 14MA of RE current.
Fig. 3 Power removed by coolant vs. tube wall temperature (solid lines) and He temperature (dashed line); the required coolant velocity (m/sec) and corresponding pressure (MPa) are indicated.
Fig. 4 The W surface temperature and maximum EUROFER temperature vs. net incoming heat flux under steady-state operation and helium cooling (u=150m/sec, P=190MPa)
Fig. 5 The W armor surface temperature vs. W armor thickness is shown for the different off-normal events in DEMO.
Fig. 6 The maximum EUROFER temperature as a function of W armour thickness for different off-normal events.

Table caption
Specifications of energy loads on DEMO FW

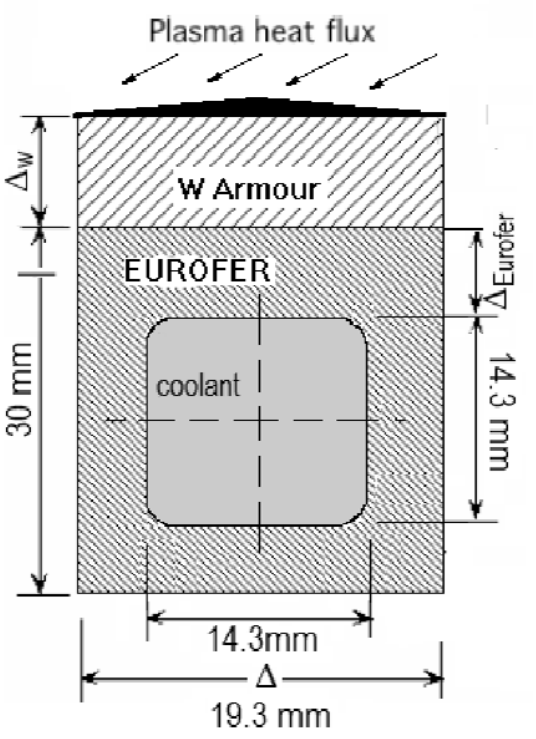

Figure 1

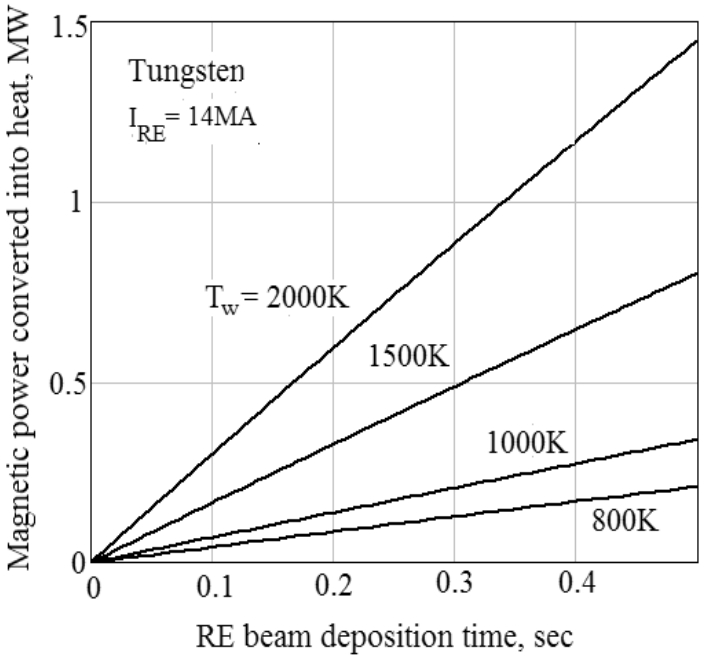

Figure 2

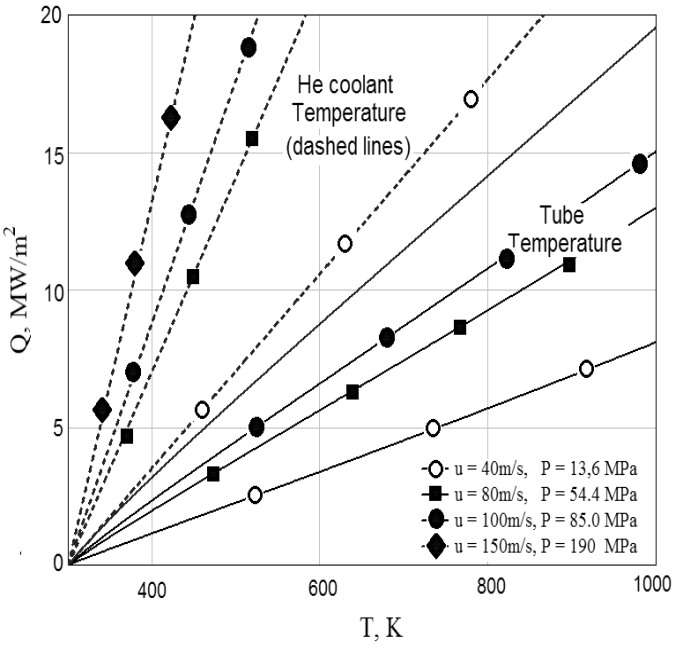

Figure 3

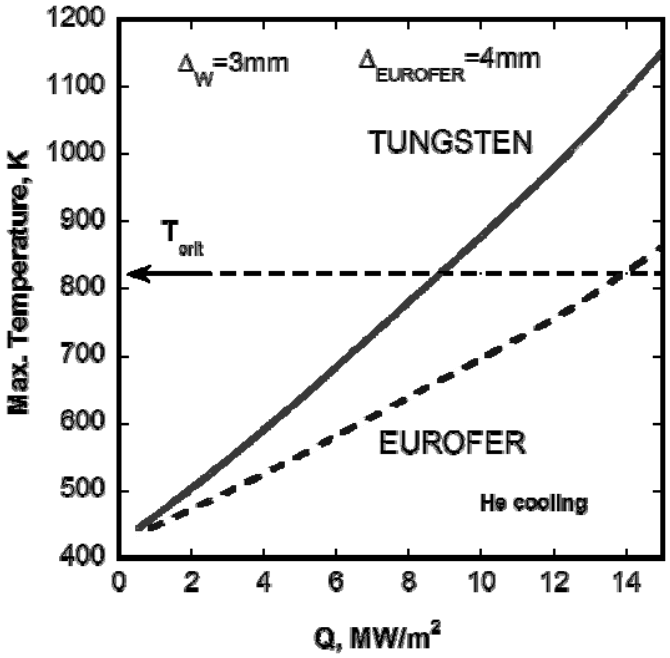

Figure 4

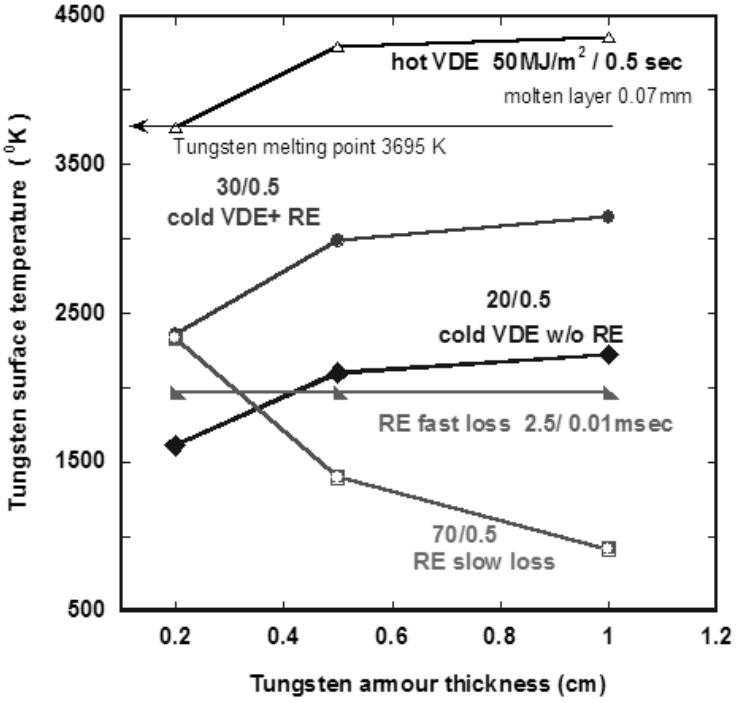

Figure 5

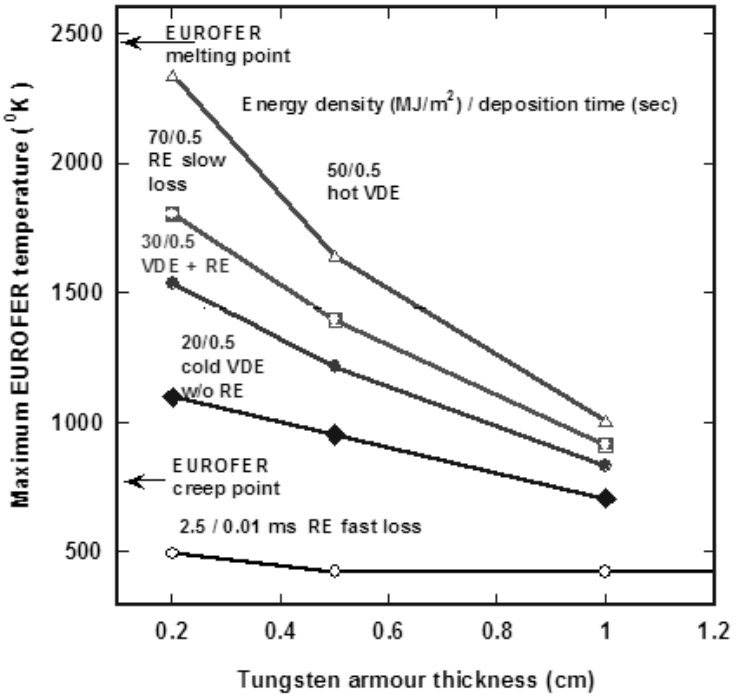

Figure 6

Table I. Specifications of energy loads on the DEMO FW

events	Removed energy, GJ	Deposited area, m^2	Deposition time, sec	Energy density, MJ/m^2
Steady-state regime	radiation +c.-exch.atoms	FW, baffles	hours	0.5-20 MW/m^2
hot VDE	$W_{th}(0.7)+40\%W_{mag}(1.2)$	~25-50	~0.5-1	~50
cold VDE w/o RE	$\sim 40\%W_{mag}(1.2)$	~25	~0.5-1	~30*
cold VDE with RE	$\sim 40\%W_{mag}(1.2)$	~16	~0.5	~600-1500*
RE slow loss	$W_{RE,\,kin}(.04)+W_{RE,mag}(\leq 1)$	~16	~0.5	≥70
RE fast loss	$W_{RE,\,kin}(0.04)$	~16	0.01msec	~2.5

* 100% of magnetic energy

II. PLASMA PLASMA FACING MATERIALS LIFTIME IN STEADY STATE DEMO OPERATION

Yu. Igitkhanov, B. Bazylev and I. Landman,
presented in the ANS 20th Topical Meeting on the Technology of Fusion Energy, TOFE, Nashwille, 2012 ; will be published in 2013 Fusion Science and Technology.

In the steady-state operation the life-time performance of functional and structural materials in fusion reactor DEMO will be limited by several processes such as a sputtering erosion, transient events and neutron irradiation. The design strategy is to determine the structure and coating thicknesses which maximize component lifetime against all lifetime limitations. The sputtering erosion of the first wall tungsten armor layer due to the plasma impact during the steady state DEMO operation is considered here. It is shown that for DEMO conditions the total sputtering erosion of W armor by the charge-exchange DT neutrals could at least reach~1mm during one year of steady-state operation.

1. INTRODUCTION

In this paper we consider some problems related to the DEMO steady-state operation, namely: 1) the plasma impact on the first wall (FW) during a long duration steady-state operation and 2) the plasma–wall interaction associated with sputtering erosion during a long pulse exposure of heat and particle flux onto the FW tungsten armor and consequent bulk plasma contamination.

For DEMO reactor a sandwich type EUROFER blanket module coated with tungsten armor was suggested for the first wall (FW) (see details in Ref.1). In steady-state operation the power and particle loads to the FW is expected due to the convective transport in the far scrape-off layer2 and can be estimated as ~ 0.5 MW/m^2 and ~2 10^{21} m^{-2}s^{-1} ,correspondingly, and the temperature in the range of ~ 100-500 eV. On divertor plates the power flux is about 10-20 MW/m^2, particles flux~5 10^{21} m^{-2} and the temperature ~ 500-1000 eV (Ref.2). To operate within an acceptable power loading level on material structure a considerable amount of energy (> 90 %) have to be removed as a radiation. Core radiation by seeding Kr or Xe impurities can be used to reduce the power flux over the separatrix to a value of about twice the L-H power threshold to preserve good energy confinement. The remaining power flux must be largely reduced by divertor radiation, e.g. from seeded nitrogen in the SOL and divertor areas.

During normal operation the erosion of the FW and baffle surface could also occur due to collisions with hot DT neutral atoms. Undergoing charge–exchange collisions with the hot ions in the pedestal region, energetic neutrals will cause excessive power loads to the FW armour surface (>> 0.5 MW/m^2), and produce a strong erosion, particularly in the vicinity to injecting ports.

In this paper we first estimate an optimal thickness of W armour (Δ_w) and the distance between cooling pipe and the EUROFER/W interlayer ($\Delta_{EUROFER}$) which allows the FW blanket module to tolerate power loads expected in DEMO without melting of armour and thermal destruction of structural material. Then, the sputtering erosion of W during the steady-state operation is calculated by taking into account the sputtering yield increase due to shallow incident angles and acceleration of incident particles in the sheath at the divertor plates.

In calculations we consider a cooling system as straight rectangular tube imbedded into the EUROFER structure as described in (Ref.1). Helium gas is taken as a coolant.

2. STEADY- POWER LOADS UNDER STEADY-STATE OPERATION

The MEMOS and ENDEP codes[3] have been employed to calculate the effect of power loading during steady-state DEMO operation. The net incoming heat flux Q under steady-state operation onto the W armour is assumed in the range of 0.5-15 MW/m^2. Such a range of Q can be expect in DEMO due to transient events like ELMs and convective radial plasma losses, associated with unstable convective cells in the SOL region during steady-state operation.

Calculation shows that under expected heat loads the surface temperature remains well below the W vaporization and melting and the heat flux into coolant below critical heat flux thus avoiding severe degradation of the heat removal capability. For incoming heat flux ≥ 10 MW/m^2 W bulk temperature approaches a soft limit of ~ 900-1050 °K. However, at this temperature range the crack formation could be expected[4]. Variation of the surface armour temperature and interlayer temperature with EUROFER thickness is shown in Fig. 1 for given Δ_W =3mm and Q=13.5 MW/m^2. To keep the W surface temperature below 730°C, the W armour thickness should be taken ≤ 3-4 mm. As it will be shown below such a thickness could be sacrificed during about three years of continuous operation by only the sputtering erosion.

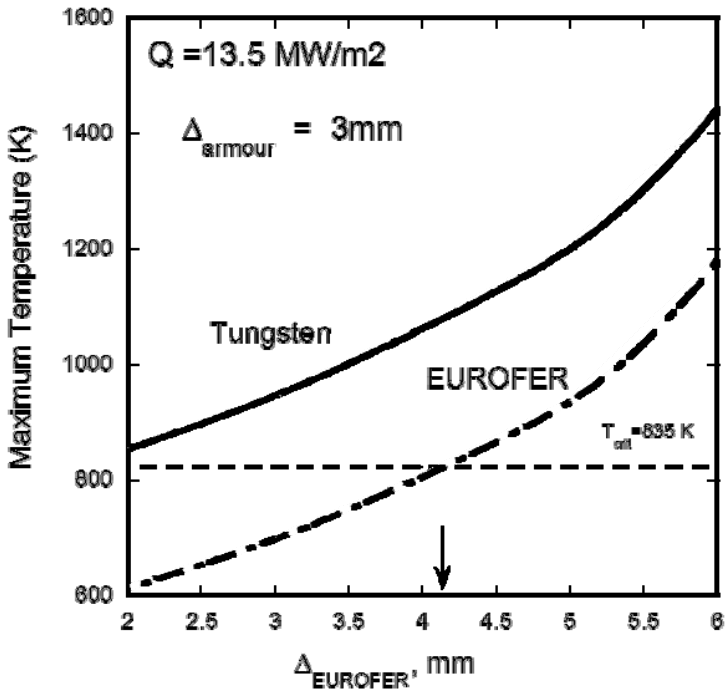

Fig. 1 Maximum temperatures of W and EUROFER vs the distance between cooling pipe and the EUROFER/W interlayer, $\Delta_{EUROFER}$). For $\Delta_{EUROFER}$ < 4.3 mm max EUROFER temperature remains below the critical value (creeping point).

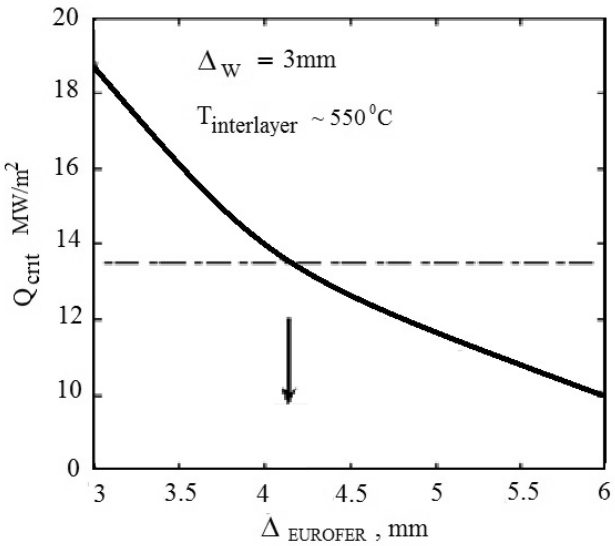

Fig. 2 . Critical incident heat flux Qcrit depending on the the distance between cooling pipe and the EUROFER/W interlayer, $\Delta_{EUROFER}$) when the maximum EUROFER temperature equals to the critical value ~550 ºC; W armour thickness Δ_w=3mm.

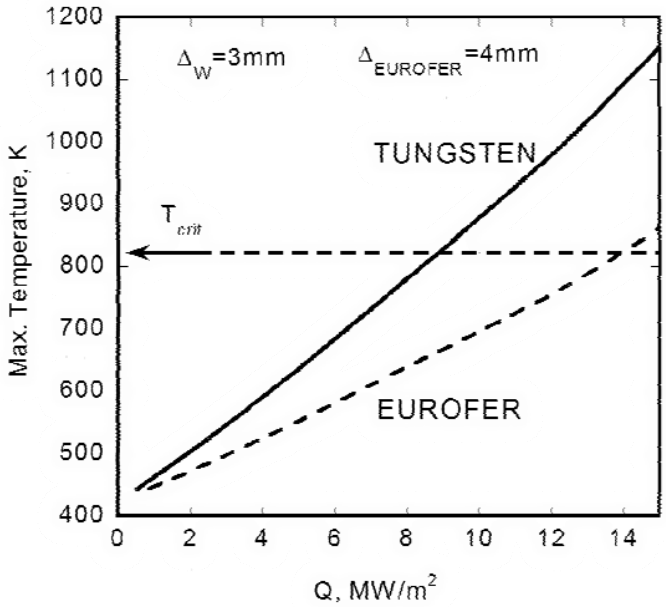

Fig. 3 W surface temperature and maximum EUROFER temperature vs net incoming heat flux Q under steady-state DEMO operation.

There will be no thermal degradation of the structural material for $\Delta_{EUROFER} \leq 4.5$ m. Fig. 2 shows heat loads and corresponding thickness of EUROFER when operation causes no thermal degradations (region below the curve). Arrow indicates the thickness value for the same case as in Fig. 1.

Calculations for various values of armour thickness Δ_w and the EUROFER thickness $\Delta_{EUROFER}$ show that the optimal are the values of Δ_w =3 mm and of $\Delta_{EUROFER}$ = 4mm. Fig. 3 shows the FW armour surface temperature and the maximum EUROFER temperature (interlayer temperature) for different incoming heat flux values Q. When Q reaches~14 MW/m^2 the interlayer temperature exceeds the critical value Tcrit. ~ 550 ºC and EUROFER can experience irremediable thermal distraction[4].

Calculations show that the volumetric heating associated with the neutrons is not particularly demanding for the first walls blanket design, whereas the surface heating is important in term of allowable temperatures and stresses.

The MEMOS code was used for evaluation of heat flux transfer through the entire module to a coolant. The Reynolds and Prandtl numbers evaluated at the mean flow temperature are Re $\geq 2\text{-}5\cdot 10^5$ and Pr $\geq$ 0.67, thus confirming the applicability of the turbulent model under DEMO conditions The required heat transport coefficient is ~ 6 kW/m^2/K and the resulting high fluid velocities are in the range of 60-190m/s depending on the removal heat flux. Under these conditions EUROFER stays at temperature ~ 550 ºC, this is needed to avoid an embrittlement under neutron irradiation. At the same time calculations show that helium coolant allows one to remove thermal power keeping the material temperatures below the EUROFER creep point and W armour below the melting point (3410 ºC).

3. SPUTTERING EROSION IN A LONG PULSE DEMO OPERATION.

The important erosion process for the FW and baffles under steady-state DEMO operation is expected to be physical sputtering, since the W surface temperature remains below the melting point and ignition of arcing is insufficient for life-time limitation under normal operation[5,6]. In our calculation we have emphasised two new important effects, which previously were ignored or approximately accounted for[7]. This is the dependence of sputtering yield on the angle of incidence and, particularly, the sheath potential effect on deviation of the distribution function of incident ions from maxwellian one. The thickness, d of plasma facing elements (e.g. the FW blanket armour, limiter, etc.) sputtered away during Δt operation time by incident particle fluxes Γ_j of different species j, can be expressed as [8]

$$d(t) = \Delta t \cdot \frac{A_t \cdot m_p}{\rho_t} \cdot \sum_j \left\langle Y_j \Gamma_j \right\rangle \tag{1}$$

where A_t is the target atomic mass (in amu), ρ_t is the target material density, $Y_j(E,\theta)$ is the sputtering yield of particle j with energy E and angle of incidence θ and Γ_j, is the flux of particles j. The brackets in (1) represent an average over the angular and energy distribution of incident particles. Thus, the precise determination of the erosion rate needs the correct form of the energy distribution function of the incident particles and the sputtering yield $Y_j(E,\theta)$. Here we present the results of erosion rate calculations taking into account deviation from Maxwellia the distribution function at the divertor plates due to the sheath acceleration and the angular dependence of the sputtering yield. Following Ref. 8 the twice averaged sputtering yield, defined as the yield averaged over the distribution of energy and angle of incidence of the projectiles, is given by

$$\overline{Y_j}\left(\frac{atom}{ion}\right) = S_0 \int_0^1 \int_{\varepsilon^*}^{\infty} \exp\left(-\frac{\varepsilon}{\beta}\left(1-t^2\right)\right) \times \exp\left[-\left(\sqrt{\frac{\varepsilon}{\beta}t^2 - \delta} - M_0\right)^2\right] \cdot tS(\varepsilon,t) \cdot \varepsilon d\varepsilon \tag{2}$$

where

$$S_0 = \frac{2E_{Th}^2}{T_i^2 F(M_0)}, \quad t \equiv \cos\theta,\ \varepsilon = E/E_{Th}, \varepsilon^* = \max(1,\delta); \quad \beta = T_i/E_{Th},\ \delta = Z_j e\varphi_0/T_i$$

Here M_0 is a Mach number of incoming particle flux (which must be taken to one at the divertor plate according to Bohm condition and to zero at the FW), $S(\varepsilon, t)$ represents, the sputtering yield for a certain energy ε and angle of incidence of the particles, θ. This dependence can be described by the revised Bohdansky formula[9] for the energy dependence and the Yamamura formula[10] for the angular dependence. Fig. 4 shows that the sputtering yield of tungsten for normal and shallow (70º) angles of Ar and Ne incidence varies in order of magnitude for high energies (≥ 1 keV).

The angular dependence becomes less pronounced after averaging over incident energy and in the case of cos-like of the angular distribution (see Fig. 5).

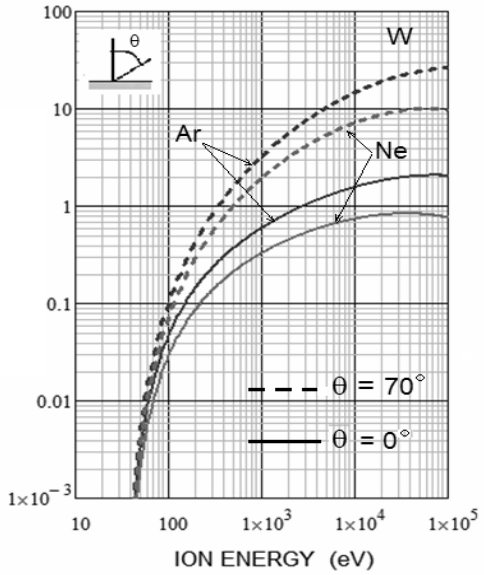

Fig. 4. W sputtering yield $Y(E,\theta)$ for two angles θ = 0º and 70º of incidence of Ar (Z=18) and Ne (Z=10) ions vs. their energy; $Y(E,\theta)$ expression is used from[9].

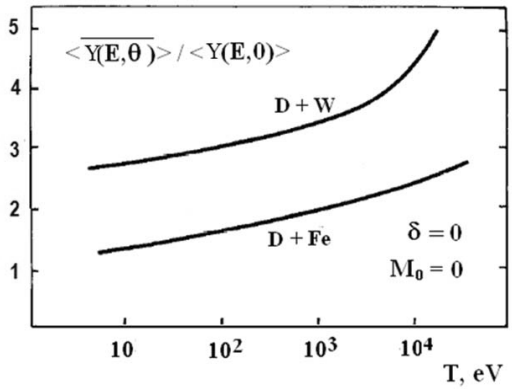

Fig. 5. Ratio of the sputtering yield of D ions over W and Fe, averaged over energy and angle of incidence to the yield averaged over energy only (i.e. for θ = 0).

The importance of the incident particles acceleration in the sheath region is demonstrated in **Fig. 6**, where the twice averaged sputtering yields for Ar ions(in different charge states Z) on W for Mach numbers M=0 (without acceleration) and M=1 (with acceleration) are compared. Substantial difference is particularly seen for the relatively low ion temperatures ($T_i \leq 100$eV).

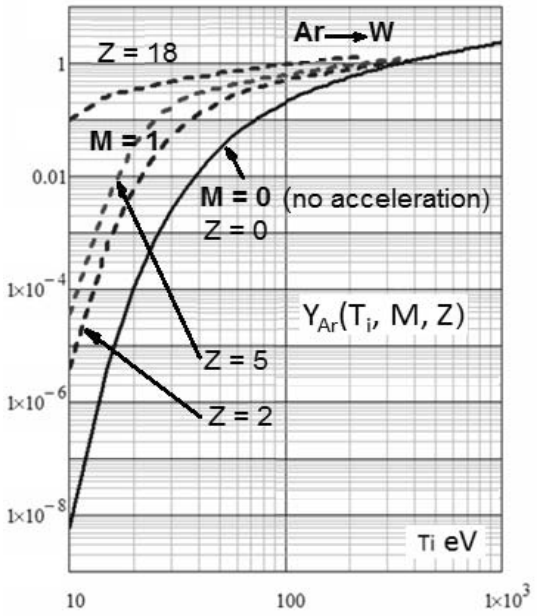

Fig. 6. W sputtering yield (twice averaged)Y (T_i,M,Z) vs. the ion temperature for Ar incident ions in the case of acceleration in the electric sheath (M=1) and without acceleration (M=0).

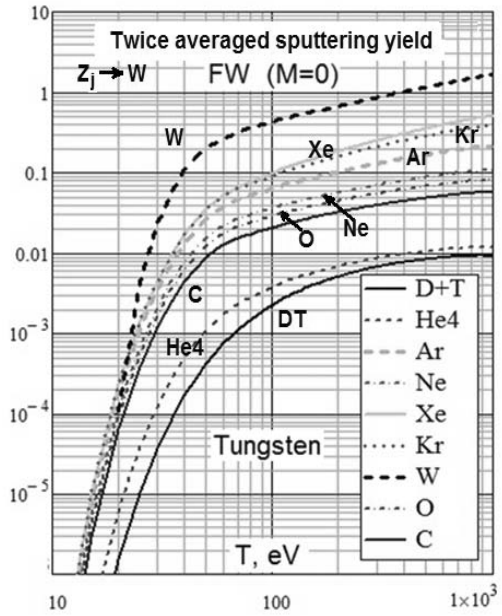

Fig. 7. W sputtering yield (twice averaged) vs. the ion temperature for various incident impurity ions in the most representative ionization charge states for corresponding temperatures.

The twice averaged values of W sputtering yields for various incident impurity ions taken at the most representative charge states at given temperature are evaluated based on Eq. (2) and data from [9,10,11] (see Fig. 7). In these calculations the case of Maxwellian distribution of incident impurity ions on the FW is assumed (M=0).

Using formula (1) the erosion rate of W armour sputtered during one year of continues operation by various particle fluxes of D+T+5%He^{+2} incident ions is calculated (see Fig. 8a for the FW and in Fig. 8b for the divertor plates). Here we are taking into account that the 'fatal' concentration of He is about 5% from the average DT plasma density. For estimates of erosion rates a total wall ion flux of 10^{24} D+T at/s is taken, which corresponds to an average flux density of 10^{17} at/cm^{2}s. Since this value remains uncertain for DEMO, we vary flux in the range of 10^{16}-10^{18} 1/cm^2/s. A seed impurity concentration of a few per cent, e.g. 2% N^{3+} (divertor seeded species) must be taken into account for the calculation of erosion rates, a spatial peaking factor (inhomogeneity of fluxes) of ~2-3 has to be assumed as well (similar to ITER).

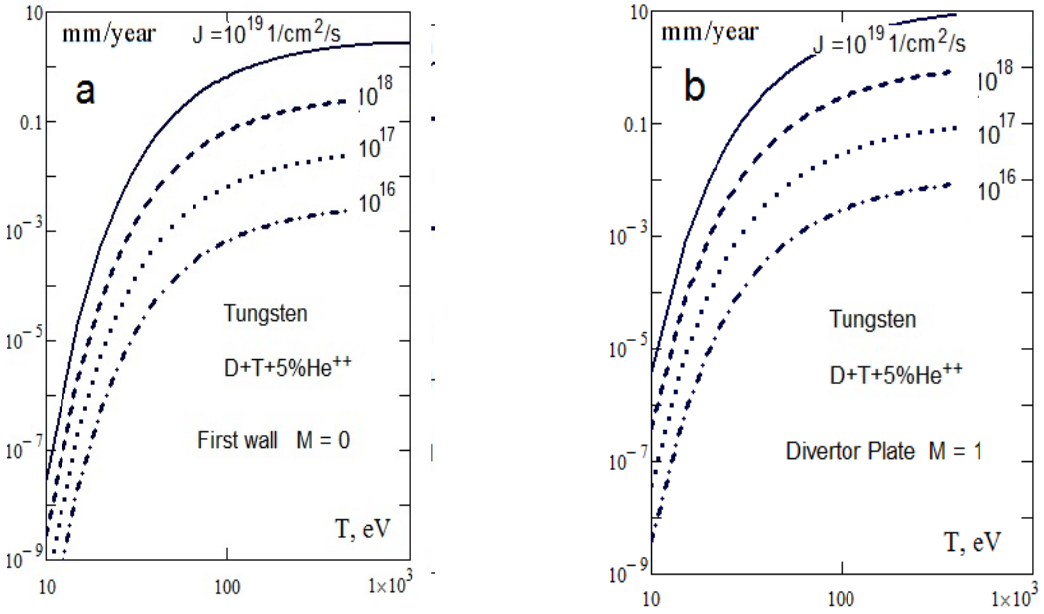

Fig.8. The thickness of the FW W armour (a) and divertor W plate (b) sputtered during one year of continues operation by various particle fluxes of D/T/5% He of incident ions J(cm^{-1}sec^{-1})

Calculations show that for envisaged in DEMO conditions the total sputtering erosion of the FW W armor by the charge-exchange DT neutrals and 5%. Helium could reach ~ 1mm during one year of steady-state operation (for particle flux of 10^{19} cm^2/s and T>100eV). Sputtering erosion from the divertor plates is about 10 times high. Note that, this result was obtained without taken into account the re-deposition of sputtered ions.

4. CONCLUSIONS

Under steady-state operation condition the FW W/ EUROFER blanket module with helium coolant can tolerate the thermal loads expected in DEMO. The minimum W armor thickness is limited by the maximum allowable temperature of EUROFER (~550 ºC). The W armor thickness Δ_w ~ 3mm and the EUROFER width $\Delta_{EUROFER}$ ~ 4mm are found optimal. The W surface temperature for Δ_w~3mm remains below the melting point and the EUROFER temperature ≤ 550 °C. For the reference case (Δ_w ~ 3mm, $\Delta_{EUROFER}$ ~ 4mm) the maximum tolerable heat flux (which does not cause thermal destructions in structural material) is about ~13.5 MW/m^2.

Estimation of erosion of the FW by charge-exchange neutrals and the divertor plates by incoming ions shows the importance of angular dependence of sputtering yield and, particularly, the sheath potential effect. We have shown that the sputtering yield increases if the sheath potential is taken into account and that the usual estimation of the sputtering yields at energy $E=3.5ZT_e$ (to account for the sheath effect) underestimates the result. It is found important to account for the angular distribution of incident light ions at low and high temperatures in order to calculate correctly the sputtering yield averaged over the distribution function of the incident particles. Calculations show that under envisaged in DEMO conditions the total sputtering erosion of the FW W armor by the charge-exchange DT neutrals and 5% Helium could reach ~ 1mm during one year of steady-state operation (for particle flux of 10^{19} cm^2/s and T > 100eV). Sputtering erosion from the divertor plates is about 10 times high (without redisposition effect).

Our results indicate that high pressure for Helium coolant in inlet is needed to achieve the required heat transfer to the coolant. This requires a big pumping power which could reduce the efficiency of the power conversions. In spite of this deficiency, helium adaptability to any operational temperature makes it very suitable for application in DEMO.

ACKNOWLEDGMENTS

This work, supported by the European Communities under the EFDA contract of Association between EURATOM and Karlsruhe Institute of Technology (KIT), was carried out within the framework of the European Fusion Development Agreement. The views and opinions expressed herein do not necessarily reflect those of the European Commission.

REFERENCES

1. YU. IGITKHANOV , B. BAZULEV, I. LANDMAN and L. BOCCACCINI, paper P1-39 in conference of PSI, Aachen, 2012 (accepted for publication in Nuclear Materials).
2. D. WARD, Provisional Parameters for a Steady-State DEMO Device, TW6-TRP-002, Culham Science Centre, UK (2006); ITER Physics Basis, Chapter 9: ITER contributions for Demo plasma development, Nucl. Fusion 47, (2007) S404; ITER DDD, WBS1.9, Physics Section 6.3, 1983;
3. B. BAZYLEV et.al, J. Nucl. Mater. 307-311 (2002) 69
4. S.PESCHANYI et al., Fusion Engineering and Design 86 (2011) 1681–1684
5. 5. YU. IGITKHANOV, B. BAZYLEV, Journal of Modern Physics, 2011, 2, 131-135; R. RAFFRAY, G. FEDERICI, Journal of Nuclear Materials 244 (1997) 85-100; G. FEDERICI et al., Journal of Nuclear Materials, 290-293 (2001) 260-265;
6. S. R. BERICH, G. FEDERICI, A. KUKUSHKIN et al., Journal of Nuclear Materials, 313–316 (2003) 388–392
7. G.F. MATTHEWS, Journal of Nuclear Materials, 337–339 (2005) 1–9
8. V.ABRAMOV, YU.IGITKHANOV et al., J. Nucl. Mater. 162-164 (1989) 462.
9. W. ECKSTEIN, C. GARCIA-ROSALES, J. ROTH at al; Max-Planck-Institut ftir Plasmaphysik Report, IPP 9/82 (1993).
10. Y. YAMAMURA, Y. ITIKAWA and N. lTOH, Nagoya University Report, 1PPJ-AM-26 (1983)
11. D. E. POST, R. V. JENSEN, C. B. TARTER, W. H. GRASBERGER, W. A. LOKKE, Atomic Data and Nuclear Data Tables 20, 397-439 (1977).

IV. Plasma Facing Materials Lifetime in Fusion Reactor: Effect of ELMs.

Yuri Igitkhanov, Boris Bazylev, Sergei Pestchanyi and Igor Landman, presented in the ANS 20th Topical Meeting on the Technology of Fusion Energy, TOFE, Nashville, 2012
manuscript number: FUSENGDES-D-12-00604

The off-normal and transient events could pose a severe tread causing a melt-erosion and thermal fatigue in functional and structural materials in fusion reactor DEMO. In this work we analyze the impact of unmitigated edge localized modes (ELMs) on the first wall sandwich type blanket module. The expected ELMs characteristics for DEMO are estimated by extrapolating predictions made for ITER and by using the scaling arguments. The tungsten and EUROFER material damage and effect of melt layer motion on the subsequent ELM loads is numerically investigated by using the MEMOS code (Bazylev,2002). It is shown that due to the ELMs repetition impact the total tungsten surface roughness will considerable grow. The magnitude of roughness after many ELMs with the heat loads stochastically distributed over the divertor surface. It is proven that the considerable alleviation of ELMs in DEMO will ultimately require. The effect of runaways and vertical displacement events is also considered under DEMO conditions.

1. Introduction

The plasma material interface in DEMO is more challenging than in ITER, due to the requirements for approximately four times higher heat flux from the plasma and approximately five times higher average duty factor [1]. We consider here the DEMO design of ~1GW of electric power, the major radius R=7.5m, the aspect ratio A=3, the toroidal magnetic field B=6T and the safety factor q_a=4.5 [2]. A sandwich type first wall (FW) blanket module made of W-clad EUROFER steel (see Fig. 1) is examined against heat loads expected in DEMO reactor due to the edge localized modes (ELMs) and off-normal events. The module consists of a helium coolant tube of rectangular cross-section within the EUROFER matrix that is used as heat diffuser [3,4]. Below we consider two types of off-normal events: a loss-of control "hot" and following a disruption "cold" vertical displacement events (VDE) and runaway (RE) generation that can occur during the current quench following a disruption. Both, VDE and RE energy deposition would affect mostly the first wall [4]. The consequent erosion due to excessive power and particle loads on plasma facing components (PFC) is expected in DEMO, particularly, because of a huge amount of poloidal magnetic energy (~1.2GJ) which will eventually dissipate in the material structure. We evaluate here the conversion of magnetic energy into heat due to mainly ohmic dissipation of return current, induced during the penetration of RE beam into the tungsten armour. Although W/EUROFER bound is of "low-activation" type, it has relatively low creep temperature (823°K) which could be the main drawback of EUROFER as a structural material. To assess proper design parameters of the FW module, calculations were performed with the Monte Carlo Energy Deposition code ENDEP together with the upgraded version of MEMOS code [6], which takes into account helium as a coolant and the RE magnetic field energy convertion into heat. The details of the RE modelling by means of ENDEP code are described in [5]

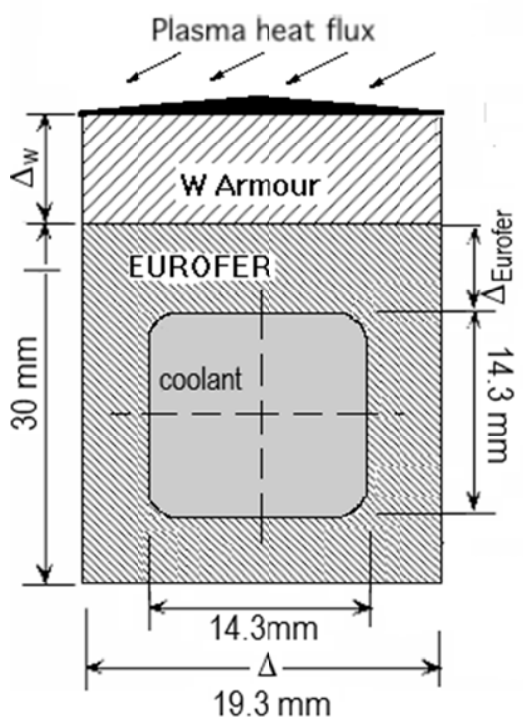

Fig. 1 Mock-up of a sandwich type W/EUROFER blanket first wall module used for the Monte Carlo MEMOS computation of the plasma impact. Helium coolant was used.

In this paper we first discuss the expected parameters of ELMs in DEMO and their effect on the tungsten armor melting and roughness formation due to the tungsten vapor pressure. Then, the effect of VDE and RE relevant to DEMO conditions will be discussed and the effect of off-normal events on the blanket module surface will be evaluated.

1. Effect of ELMs

The ELM characteristics in DEMO can be assessed based on scaling arguments by extrapolating data envisaged for ITER [1,6] and the large-scale tokamaks. In ITER the thermal energy ΔW_{ELM} realized during unmitigated ELMs is expected to be about ~20 MJ. 2/3 of this energy deposits in outboard diverter and the deposition time is about 0.3ms (rising phase) and 0.6ms (decay phase). The peak energy on outboard diverter is about 0.5-4MJ/m^2. For extrapolation to DEMO one can use the fact that the Type I ELM frequency scales as $f_{ELM} \sim(\tau_E)^{-1/7}$, where τ_E is the energy confinement time. The confinement time for the H-mode ELMy discharges τIPB98(y,2) [1] is ~6.47sec for DEMO conditions [2], which exceeds ~1.8 times the confinement time for ITER. Consequently, the ELM frequency in DEMO is expected to be about 0.8Hz, which is lower than for ITER (~2Hz)[7]. The power loading per each ELM, P_{ELM}, for fusion reactor can be estimated based on assumption, that $P_{ELM} \geq P_{LH}$, where P_{LH} is the threshold power for L to H transition. For DEMO this implies that $P_{ELM} \geq$ 300MW, by using the existing empirical formula for P_{LH} [1]. Thermal energy ΔW_{ELM} can be estimated as P_{ELM}/f_{ELM} and is about 100MJ for unmitigated ELM. We further assume that the shape of ELM power loading at the mid-plane is the same as it is expected in ITER: the decay phase is twice longer than the rising phase. The full width at half maximum varies and for the case of vertical divertor plate with incident angle of B ~20º is assumed about 0.05m. In the case of a horizontal plate (with the incident angle ~ 5º) it is about 0.02m (similar to ITER). The ELMs deposited area on the plane can be estimated as ~2πRΔ, where Δ depends on the magnetic

density load will expected in the range of 12-17MJ/m^2 over the deposition time about 0.5-1ms (in rising phase) and 1-2 ms (in decay phase). The heat loads typical of single type I ELMs could result in melting and evaporation of W armor surface and in a vapor shield formed in front of the armor [9]. Melt motion produces surface roughness that usually significantly exceeds the vaporization erosion per one ELM. We evaluate the melt layer formation on tungsten armor surface due to the ELM loads expected in DEMO. Due to the ELM repetition the total roughness may accumulate and get rather high. The magnitude of roughness after many ELMs with the heat loads stochastically distributed over the divertor surface is simulated. The heat flux profiles of Type I ELMs in experiments show a clear peak near the separatrix strike point (SSP) with random spatial variations of SSP position and of heat flux for sequential ELMs [10]. It seems justified to assume that the position of SSP at the divertor plate stochastically moves obeying the Gaussian distribution, with the dispersion δ up to 0.02 m. The influence of the [jxB] force on the melt motion is not considered here because of rather uncertain value of halo current j in DEMO. The simulation of the melt motion layer in the case of DEMO W armor is similar to calculations done previously for ITER in [11] For multiple events the total erosion is evaluated by direct simulation of each ELM impact on the eroded surface produced by previous ELM. Several scenarios for single and repetitive ELMs are modeled with the target width of 0.06m. For many ELMs the case with fixed SSP position is compared with that of the SSP Gaussian distribution of δ = 0.02 m. The profiles of heat load on the plate and plasma pressure are calculated as described in [11]. It is obtained that for reference scenario (~12MJ/m^2 and τ_{ELM}~0.5ms) the depth of melt pool is always below 80 μm and the re-solidifies after the end of ELM within 2-2.5 ms, due mainly to radiative losses. The single ELM WELM from 1-2 MJ/m^2 already produces melting without evaporation and surface roughness after re-solidification is of small fractions of micron, due to the melt motion with melt velocity V less than 0.1 m/s. For the reference case the vapor shield forms and thus the pressure gradient becomes essential. The magnitude of surface roughness is of 0.1-0.3μm (~60 μm /660), V of 0.5 m/s, and the evaporation thickness of 0.015 μm (~10μm/660) as follows from Fig 2. The [jxB] force could intensify the melt motion and will be estimated in future work. Profiles of surface roughness after N series of ELMs are shown in Fig. 3 for the reference case. At fixed SSP, the crater depth reaches 50 μm after 660 ELMs (~10μm due to the evaporation). The Gaussian distribution of SSP with δ=0.02 m results in significant decrease of the crater depth: down to 10 μm and the evaporation results up to 2 μm. The melt motion increases the total erosion by a factor not larger than 5.

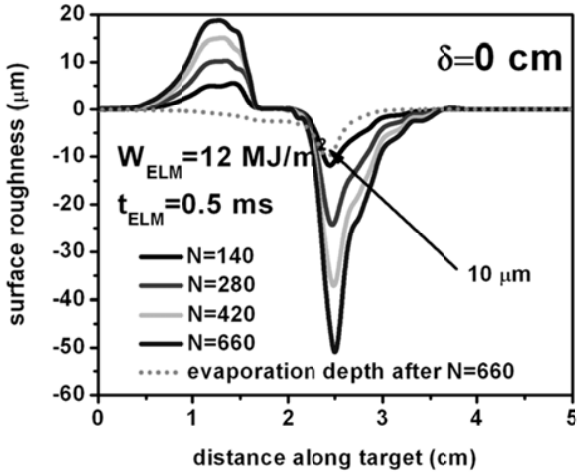

Fig. 2. Effect of multiple ELMs with a fixed strike point position (δ=0), pressure gradient acts along the plate surface. N is the number of repetitive ELMs.

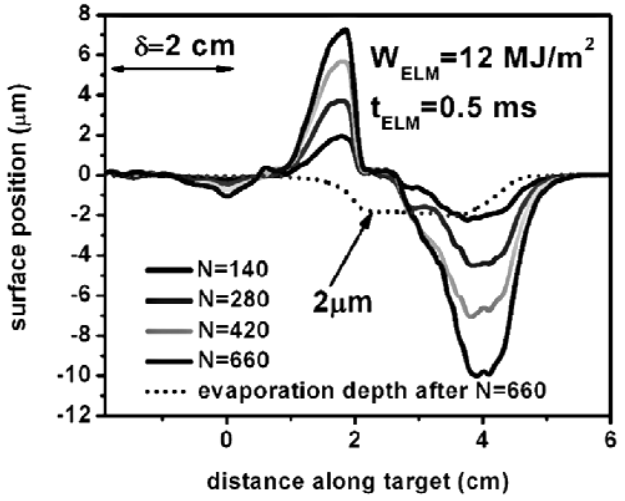

Fig. 3. Surface roughness after N ELMs for the SSP Gaussian distribution with δ = 2 cm. N is the number of repetitive ELMs.

The simulations demonstrate that for the Type I ELMs in DEMO with W_{ELM} ~12 MJ/m^2 the pressure gradient of the plasma shield is mainly responsible for an intensive melt motion of tungsten target with the melt velocities up to 0.5 m/s. For many ELMs at fixed SSP the maximum craters depth exceeds the evaporation thickness by a factor less than 5. Assumption on stochastic motion of SSP along the target surface essentially decreases the total erosion

3. Effect of off-normal events

The characteristics of off-normal events in DEMO can also be assessed based on scaling arguments by extrapolating data envisaged for ITER.. In the case of VDE which may occur due to accidental loss of control in DEMO, we assume that ≤ 2GJ (~0.7GJ of plasma thermal energy and ~1.2 GJ of magnetic energy) will eventually deposit on the FW structure. The resulting energy density can be estimated in the range of ~50-100 MJ/m^2, which includes toroidal and poloidal peaking factors similar to ITER and assumption that the deposited area~2πRd is about 25-50m^2 corresponding to toroidally continuous band d = 0.5-1m and the DEMO major radius R=7.5m. In this case of accidental control loss the plasma column drifts toward the wall with the resistive growth time of vessel structure, which we assume in DEMO similar to ITER - of the order of ~0.5-1sec. In the case of 'cold' VDE, when vertical instability arises after thermal quench, current channel moves towards the wall during current decay and deposits remaining energy to the FW. We take in our calculations the worst-case assumption that the magnetic energy deposits to the FW surface band of 25m^2 over ~ 0.5-1 sec. Since the stored plasma energy in DEMO is by at least a factor of two higher than that in ITER [1], the kinetic energy of REs in DEMO can be assumed as Wkin~20MJ x 2π·40 MJ [3]. Slow RE loss is accompanied by transformation of magnetic energy in RE kinetic energy. Fast RE losses triggered by major MHD modes will occur on the Alfven time scale of τ_{MHD}~R/c_A~15μs, where R=7.5m is plasma major radius and c_A~6.105 m/s is Alfven velocity for poloidal field B_p~0.4T [2]. During this short time the plasma column can be considered stationary as whole. RE velocity normal to the FW surface will be determined by plasma convection on MHD time scale Vperp~a/τ_{MHD}~2· 10^5 m/s, where a=2.5m is the minor radius. Thus, the incident angle (on axisymmetric wall) is Vperp/c~10^{-3} and RE SOL thickness is ΔSOL~2πqRV_{perp}/c~0.27 m, q~3 is the safity factor. One can assume that during the fast loss magnetic energy is not transferred

is about $H\sim(2a\Delta_{SOL})^{1/2}\sim1$m. It is likely that plasma will be toroidally asymmetric during this event with large n=1 perturbation of its shape and thus the worst case assumption is that all RE will be deposited on a single or a few toroidal FW section. If deposition occurs on 1/3 of the toroidal circumference, then the wetted area can be estimated as $\sim1/3\cdot(2\pi R)\ (2a\Delta_{SOL})^{1/2}\approx16m^2$. Therefore, the RE kinetic energy density of ~50-70MJ/m^2 is expected in DEMO FW. We assume that the total RE energy varies in the range of 30-100 MJ/m^2 keeping in mind that part of the poloidal magnetic energy could eventually also be converted into RE kinetic energy [6] and (like in JET) a large fraction~40% could dissipate in the plasma-coupled conducters. The RE current can be estimated as Ire ~10-15MA, which is about ≤70% of the total plasma current (similar to estimations for ITER). In our calculations we also assume that the energy deposition time of RE is in a range of 0.05-1s. This roughly corresponds to the loss time of high-energy REs because their drift orbits intersect the wall in resistive time scale and this time depends on the thickness of the wall structure. Specifications of energy loads on DEMO FW are summarized in paper [4].

Calculation where performed for armor thickness Δ_w = 3mm and for EUROFER thickness $\Delta_{EUROFER}$ = 4mm (see Fig. 1). Fig. 4 shows the surface temperature of the tungsten armor and the maximum EUROFER temperature (interlayer temperature) for different heat loads in steady-state regimes of operation. Both temperatures increase with the increase the heat load. For heat loads above14MW/m^2 the EUROFER temperature exceeds the creep point T_{cr} = 823K and EUROFER loos its creep strength [6]

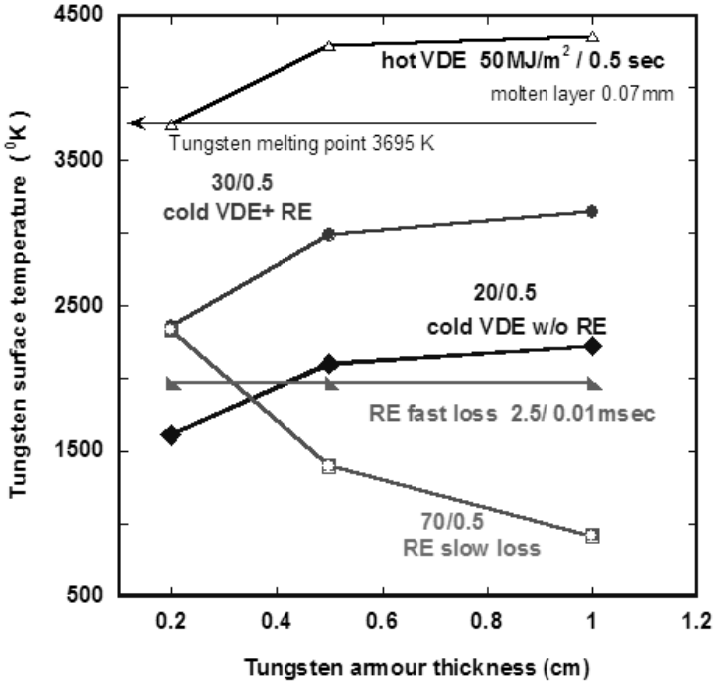

Fig.4**.** The W armor surface temperature vs. W armor thickness is shown for the different off-normal events in DEMO.

Calculations show that in the range of heat fluxes 0.5-12MW/m^2 and under helium cooling conditions the W armour thickness Δ_w=3mm is optimal - it does not melt and protects EUROFER from excessive heating. As it was shown [4] this W thickness is sufficient to tolerate about three years of continuous reactor operation by taking into account only the sputtering erosion. Fig.5 shows the maximum of EUROFER temperature depending on W armor thickness.

Calculations show, that in the case of disruption with the hot VDE the energy deposition into the armor will cause strong surface melting up to 0.07mm and evaporation up to a few mm. In the case

Calculations show, that in the case of disruption with the hot VDE the energy deposition into the armor will cause strong surface melting up to 0.07mm and evaporation up to a few mm. In the case of cold VDE with or without RE tungsten temperature remains below the melting point. The same found for RE impact. Both slow and fast RE loss will not cause the melting of W armor surface, although the wetted area for RE is smaller.

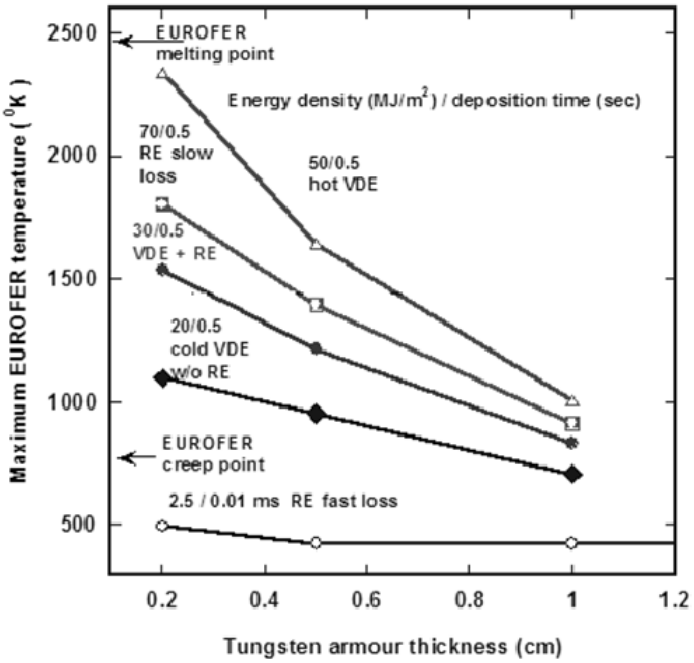

Fig. 5. The maximum EUROFER temperature as a function of W armor thickness for different off-normal events.

In the case of RE fast losses, they depositing almost all kinetic and about 40% of magnetic energy into armour, the W surface temperature does not exceed~2000 K because of very short deposition time~0.01ms. In the all cases (except for the RE slow loss) the armor temperature is quite independent on armor thickness, because heat deposition takes place in a thin surface layer. In the case of the RE slow loss heat deposition occurs deeper in armor and heating time becomes comparable with heat diffusion time for W thicknesses ≤ 1cm. This explains the W temperature decrease with increasing the armor thickness. The maximum EUROFER temperature drops with increasing the W armor thickness (see Fig. 5) and does not melt for the all considered cases.

4. Conclusions

The simulation show that for the ELMs with W_{ELM} ~12 MJ/m^2 the pressure gradient of the plasma shield is mainly responsible for an intensive melt motion of tungsten target. The corresponding melt velocities is ~0.5 m/s and the surface roughness about 0.1 μm. Due to the small melt velocity and the small re-solidification time of a few ms the melt splashing does not develop therefore all mass losses are due to target evaporation. For many ELMs, at fixed SSP the maximum crater depth exceeds the evaporation thickness by a factor less than 5. Assumption on stochastic motion of SSP along the target surface essentially decreases the total erosion.

The calculations of off-normal events expected in DEMO show, that in the 'hot' VDE case the energy deposition into the W armor is rather shallow (~ nm) which causes surface melting and

evaporation. In the 'cold' VDE case the W/EUROFER structure can marginally tolerate the energy loads. The RE fast losses does not cause the W armor melting because of a very short exposure time ~0.01ms. In the case of RE slow losses electrons deposit their energy (magnetic and kinetic) deeper in armor layer, and that explains the W temperature decrease with increasing the armor thickness. In the all cases (except for the RE slow loss) the armor temperature is quite independent on armor thickness, because heat deposition takes place in a thin surface layer. In the case of the RE slow loss heat deposition occurs deeper in armor and heating time becomes comparable with heat diffusion time for W thicknesses ≤ 1cm. This explains the W temperature decrease with increasing the armor thickness. The maximum EUROFER temperature drops with increasing the W armor thickness (see Fig. 5) and does not melt for the all considered cases.

Acknowledgments
This work, supported by the European Communities under the contract of Association between EURATOM and Karlsruhe Institute of Technology, EURATOM and CCFE, was carried out within the framework of the European Fusion Development Agreement. The views and opinions expressed herein do not necessarily reflect those of the European Commission).
One of the authors (Yu. I) is acknowledged L. Boccaccini for using his model of the DEMO first wall blanket module.

References
[1] ITER Physics Basis, Chapter 9: ITER contributions for Demo plasma development,
[2] D. Maisonnier et al., Nucl.Fusion 47 (2007) 1524
[3] Yu. Igitkhanov, B. Bazylev, Fusion Science and Technology, 60 (1) (2011), 349.
[4] Yu.Igitkhanov. B. Bazylev, Fusion Engineering and Design, 87, Issues 5–6, 2012, 520
[5] B. Bazylev et.al, J. Nucl. Mater. 307-311 (2002) 69
[6] A. Loarte, V. Riccardo et al., Preprint EFDA–JET–PR(10), 23, 2010
[7] M. Sugihara, ITER, private communication
[8] Yu. Igitkhanov, O. Pogutse, H. Wilson et al., Contributions to Plasma Physics, 42, Issue 2-4, p.272, 2002
[9] H.Wuerz et al., J.Nucl.Mater. 290-293 (2001) 1138.
[10] A. Hermann et al., J. Nucl. Mater. 313-316 (2003) 759.
[11] B.Bazylev, G. Janeschitz, I. Landman, S. Pestchanyi in 30th EPS Conference on Contr. Fusion and Plasma Phys., St. Petersburg, 7-11 July 2003 ECA Vol. 27A, p-2.44

V. Efficiency of Water and Helium coolant in Fusion Reactor Blanket

Yu. Igitkhanov , B. Bazylev, R. Fetzer

(manuscript is under preparation for publication)

1. Introduction

The proper choice of coolant in the FW blanket module is important for a Fusion Power Plant DEMO operation. The coolants which will be here considered are 1) water in different operational temperature intervals (low(~100-200°C), in Power Work Reactor range (PWR) (~280°C-320°C) and in supercritical stage (>374°C)) and Helium gas. Water allows to reach high **heat transfer coefficients,** $h \equiv q[W/m^2] / \Delta T°K$ and presents high thermal capacity and sufficiently high density, that allow the transport of heat with low difference of temperatures and using relatively small volumes of coolant. Water heat capacity is under normal conditions c_p=4200 J/(kg·K). Water is, however, limited in temperatures: to avoid vapour transition the high pressure is required for with the selected temperature level (at PWR temperature level up to 15MPa). Beyond the pressure of ~ 22MPa and temperature ~ 374°C, water exists as supercritical fluid (**see Fig.1**).

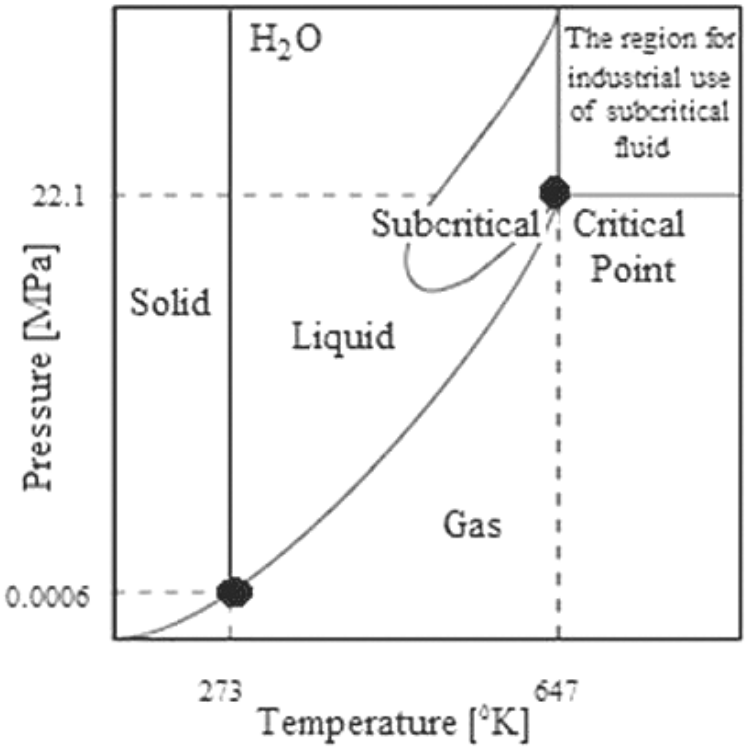

Fig.1. Phase diagram for water

The disadvantages of water as a coolant are mostly in the poor compatibility with other materials used in the fusion reactor, e.g. chemical compatibility with usual breeders/multipliers like Li, PbLi and Be. Reaction with Li is violent, less dangerous with PbLi. With Be at temperature higher than~600°C the reaction with steam is exothermic, with H production; this constitutes a serious safety issue for a reactor. Water reacts at high temperature also with other metals that could be used in the reactor (like steam with tungsten [1]) causing H release, too. Water is also responsible of corrosion with steel and this is particularly enhanced if supercritical water is used. Other issue is the mismatch of temperature windows with structural materials used in fusion, like the ferritic, ferritic-marthensitic steels. The max temperature of water (in PWR conditions) (~280°C-320°C, is too low related to the lower range suitable for these materials. Tungsten has a body-centred cubic lattice structure and exhibits very low ductility at room temperature. In fact, the DBTT tends to increase under irradiation up to temperatures related to PWR water conditions. The ductile to-brittle transition temperature can be reduced by alloying. In any case, to exploit the exceptional coolant properties of water (feature that could be very favorable for the divertor, in which huge heat fluxes strike to the target plates) a combination with suitable structural/heat materials has to be selected. Of the few possible materials with exceptional thermal properties that maybe be used for divertor application, CuCrZr could be used only at low temperature level (if capable to withstand 30 dpa that is questionable) and W/W-alloys (questionable under irradiation) are not compatible with water. New classes of suitable structural materials are requested that can withstand heat fluxes >10MW/m^2 and neutron damage at least of 30 dpa.

Water plays an important role also in the neutronic balance of the FPP. It moderates the neutrons and contributes to the parasitical absorption of neutrons. It should be considered carefully in the neutronic analysis, but possible working points exist and concept of breeding blanket have been proposed (both with PbLi and ceramic/Be).

Water has also issues with tritium. Permeation and isotopic exchange of T in water can cause issues to decontaminate the coolant water in the fusion reactor.

Considering all these arguments, it can be understand why only few concepts of fusion reactors with water cooling are considered. The only “under development” concept is the Japan Demo [2], a solid breeder blanket with water cooling; the conditions are at supercritical water technology, namely 25 MPa at 380°C, for the blanket and low pressure/temperature, namely 4 MPa at 200°C; in divertor. In EU a water cooled concepts, the Model A combining the Water Cooled Lithium Lead blanket with a water cooled divertor [3], was proposed at the beginning of the PPCS and successively dropped in favor of a Helium Cooled Lithium Lead; the coolant conditions were 15.5 MPa, 285-325°C in blanket, and 4.2 MPa, 140-167°C in divertor.

Helium gas has the best compatibility with all the materials used in the fusion reactor. Furthermore, it can be adapted to a wide range of temperature windows to cope with almost all the materials; in addition is suitable for very high coolant temperature increasing the efficiency of the power generation cycle. Howewer, as a gas its cooling properties are poor if compared with water. The low density can be partially compensated by using it at high pressure (usually 8-10 MPa). To achieve **higher heat transfer** required for cooling plasma surface component, high velocity should be achieved with increasing of pressure drops. A big issue is the huge pumping power necessary to circulate it in the system. This reduces the efficiency of the power conversions, partially nullifying the advantage of higher coolant temperature. Still suitable working points can be found, if it is possible to design blanket for pumping power lower than 5% (of the extracted heat) accepting also <10% in the divertor cooling.

The power imparted into a fluid or gas will increase the energy of the coolant per unit volume. Thus the power relationship is between the conversion of the mechanical energy of the pump mechanism and the coolant elements within the pump. In general, this is governed by a series of simultaneous differential equations, known as the Navier-Stokes equations. However a more simple

equation relating only the different energies in the coolant, known as Bernoulli's equation can be used. Hence the power, P, required by the pump: $P = \Delta p\ Q/\eta$, where ΔP is the change in total pressure between the inlet and outlet (in Pa), and Q, the fluid flow rate is given in m^3/s, $Q=v \cdot S$. The total pressure may have gravitational, static pressure and kinetic energy components; i.e. energy is distributed between change in the fluid's gravitational potential energy (going up or down hill), change in velocity, or change in static pressure. η is the pump efficiency, and may be given by the manufacturer's information, such as in the form of a pump curve, and is typically derived from either fluid dynamics simulation (i.e. solutions to the Navier-stokes for the particular pump geometry), or by testing. The efficiency of the pump will depend upon the pump's configuration and operating conditions (such as rotational speed, fluid density and viscosity etc.)

From a neutron point of view Helium is ideal as it is does not interact with neutrons, however large void fraction can be produced in the breeding zone for helium circulation increasing the volume (and so the radial thickness) of the in-vessel components (i.e. manifolds). This void fraction makes difficult also to accomplish an effective shielding function with the in-vessel components; e.g. the pipes are transparent for neutron and special design is required (i.e. dog legs) to avoid neutron streaming. Again, this results to an increase of radial-built thickness of in-vessel components.

Extraction of tritium from He is not difficult, however the safety risk related to the T permeation in components like steam generators, can require very strict requirements on the max T partial pressure in the coolant that could penalize largely the system under an economical point of view and maybe jeopardise feasibility of necessary coolant purification systems or anti-permeation barriers.
Helium cooled divertors has been proposed mainly in order:
a) to use the same coolant as the blanket in FPP concepts with helium cooled blankets;
b) to avoid the presence of water that is not compatible with some breeders (see above);
c) to reach high temperature in order to integrate with high efficiency~17% of the fusion power collected in the divertor area in the plant power generation system.

Helium can achieve easily these plant requirements. Issues are, like for water coolant, the absence of materials suitable to achieve the structural and heat requirements of the divertor, namely high pressure coolant containment, with >10 MW/m^2 heat removal at a neutron damage of at least 30 dpa.

The big disadvantage of helium coolant is the relatively low **heat transfer coefficient** that can be achieved by conventional pipe cooling. It is necessary to develop special cooling technology based on parallel cooling, with turbulence promoters like pin/fins or surface impingement through small holes. All these technologies causes high pressure drops (i.e. large pumping power) and complicate geometries (hence complicate manufacturing). Examples of development of this component can be found in [4] and [5].

The availability of Helium remains unclear. In spite of all the issues listed here, almost the half of the worldly proposed FPP concepts makes use of Helium as coolant: in EU the Model A (HCPB blanket with an High Temperature Helium Cooled, HTHC, divertor) [6] and AB (HCLL blanket with HTHC divertor) [7] are candidate for ITER TBM and DEMO. Another EU (and US) concept, the Dual Coolant Lithium Lead [8, 9], uses Helium for cooling the steel structures (~50% of the total cooling).

Calculations of thermo-physical properties of the sandwich type W/ EUROFER first wall module under DEMO conditions have been completed by means of ENDEP and MEMOS code. The maximum themperature of W armor, EUROFER and cooling pipe for different incoming heat flux have shown in Fig. 2 and Fig. 3 in cases of helium and water coolants.

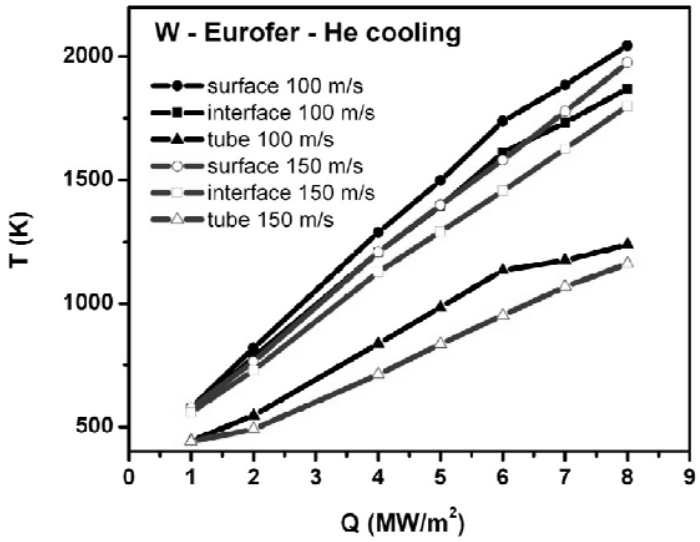

Fig.2. The maximum themperature of W armor, EUROFER and He cooling pipe for different incoming heat flux; the sandwich type W/ EUROFER first wall module under DEMO conditions.

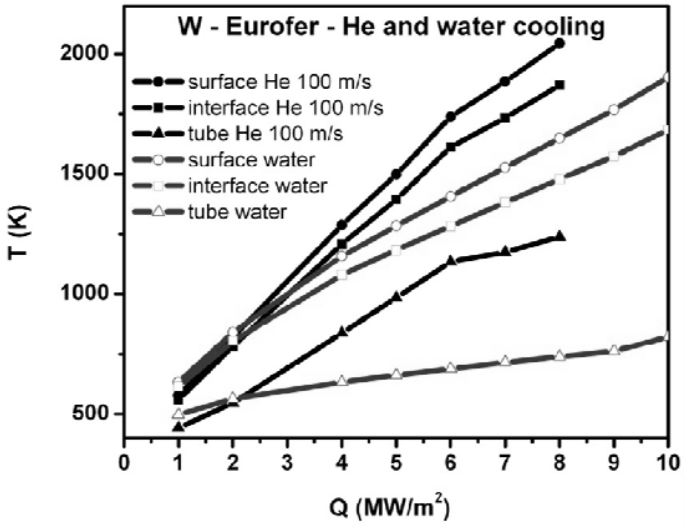

Fig.3. Comparison of the maximum themperature of W armor, EUROFER and He/Water cooling pipe for different incoming heat flux; the sandwich type W/ EUROFER first wall module under DEMO conditions.

Conclusion

Summarize, one can say, that Water remains the best coolant, but issued in compatibility with other fusion materials, make is use in a FPP very challenging. Helium has worst cooling capability, requires large volumes and causes high power pumping; however, his compatibility with all the reactor materials and adaptability to any operational temperature makes it very suitable for fusion application.

In this paper we analyse the FW sandwich type blanket module with imbedded water or helium cooling tube.

• The effect of pulsing on the first wall of a future fusion power plant is manifested mainly as thermal fatigue of the structure. Due to pulsing the temperature cycles result in varying stress in the first wall which is lifetime limiting as opposed to a steady-state mode where the number of heat-up–cool-down cycles is negligible. A series of analyses have been carried out on a "generic" DEMO outboard first wall using different parameters. The estimated lifetime from thermal fatigue point of view has been calculated. Both water and helium cooling have been considered. The effect of wall thickness between the channels and the front face as well as the coolant inlet temperature has been investigated and compared for both coolants.

• A pulsed version of DEMO with 8 h long pulses would have 1095 heat-up–cool-down cycles in a year if it operated 365 days per year [2]. The results show that from a thermal fatigue viewpoint, the lifetime of pulsed DEMO outboard FW water-cooled designs allow for a significantly higher number of cycles than helium within the limitations of the analysis. Due to the high temperatures in the helium cooled model plastic deformation can occur which is not desirable. More data is required in respect of fatigue of Eurofer 97, including irradiation effects; the effect of thermo-mechanical fatigue and non-zero mean stress. The parameters in the Coffin–Manson formula could be useful for non-zero mean stress calculations, but they need to be measured and/or calculated. The presented results are principally dominated by the effect of thermal pulsing. However the means of support can influence both the mean and alternating stress and strain. Other thermal effects like creep, irradiation creep, creep fatigue, the effects of over-power and under-power transients during a pulse have to be covered in future works. In some of these models, the wall thickness was very small. Due to the plasma interaction, the first wall will be eroded from the outside (armour was not assumed in this work), and also due to water corrosion there are likely to be problems arising inside the coolant channels. More research should be carried out to find low activation steels (or coolant additives adequately stable in the neutron radiation field) that can withstand corrosion if water cooling is considered. The corrosion problems tend to favour the helium cooling designs. The developed finite element model is parametric and it is easy to run the model for different geometry, coolant velocity or heat load for instance, therefore it can be used to create a parameter sensitivity map which could be useful information for the system code PROCESS.

References

[1] G.R. Smolik, K.A. McCarthy, D.A. Petti, K. Coates, Hydrogen generation from steam reaction with tungsten, Journal of Nuclear Materials 258-263 (1998) 1979-1984.
[2] S. Suzuki, K. Ezato, T. Hirose, K. Sato, H. Yoshida, M. Enoeda, M. Akiba, First wall and divertor engineering research for power plant in JAERI, Fusion Engineering and Design 81 (2006) 93-103
[3] P. Sardain, B. Michel, L. Giancarli, A. Li Puma, Y. Poitevin, J. Szczepanski, D. Maisonnier, D. Ward, U. Fischer, P. Pereslavtsev, A. Natalizio, J. Collen, A. Orden Martinez: Power plant conceptual study WCLL concept, Fusion Engineering and Design 69 (2003) 769-774.
[4] P. Norajitra, R. Giniyatulin, V. Kuznetsov, I.V. Mazul, G. Ritz, He-cooled divertor for DEMO: Status of development and HHF tests, Fusion Engineering and Design 85 (2010) 2251–2256
[5] M.S. Tillack, A.R. Raffray, X.R. Wang, S. Malang, S. Abdel-Khalik, M. Yoda, D. Youchison, Recent US activities on advanced He-cooled W-alloy divertor concepts for fusion power plants, Fusion Engineering and Design 86 (2011) 71–98
[6] S. Hermsmeyer, S. Malang, U. Fischer, S. Gordeev, Lay-out of the He-cooled solid breeder model B in the European power plant conceptual study, Fusion Engineering and Design 69 (2003) 281-287
[7] A. Li Puma, J.L. Berton, B. Brañas, L. Bühler, J. Doncel, U. Fischer, W. Farabolini, L. Giancarli, D. Maisonnier, P. Pereslavtsev, S. Raboin, J.-F. Salavy, P. Sardain, J. Szczepanski, D. Ward: Breeding blanket design and systems integration for a helium-cooled lithium–lead fusion power plant, Fusion Engineering and Design 81 (2006) 469–476
[8] P. Norajitra, L. Bühler, U. Fischer, S. Gordeev, S. Malang, G. Reimann: Conceptual design of the dual-coolant blanket in the frame of the EU power plant conceptual study, Fusion Engineering and Design 69 (2003) 669-673

[9] S. Malang, A.R. Raffray, N.B. Morley, An example pathway to a fusion power plant system based on lead–lithium breeder: Comparison of the dual-coolant lead–lithium (DCLL) blanket with the helium-cooled lead–lithium (HCLL) Fusion Engineering and Design 84 (2009) 2145–2157

VI. On the generation of Runaway Electrons during Massive Gas Injection

Yu. Igitkhanov, presented on 17th Joint EU-US Transport Task Force Meeting_Padova - September 3-6, 2012.; published in Contributions to Plasma Physics , Volume 52, Issue 5-6, pages 460–464, June 2012

Highly energetic runaway electrons are able to penetrate the electron shell of partly ionized heavy ions during collisions, for which reason they may be scattered by a positive charge effectively larger than that of a shielded nucleus. This effect increases the Coulomb cross section and can be treated via an effective ion charge $Z_{eff}(\varepsilon_{kin})$that depends on the energy of the incident electrons ε_{kin}. The increase of effective charge number with increasing electron energy in multi-component plasmas renders qualitatively the same result as high Z_{eff} Coulomb plasmas. Since the generation rate of runaways depends on Z_{eff}, its production during the mitigation of disruptions by massive gas injection could in some cases decrease owing to a heavy impurity concentration in the boundary tokamak plasma. This may explain why it has been observed that the runaway's avalanche is suppressed at electron densities below the so-called "Rosenbluth density".

1 Introduction

The multiplication of runaway electrons (RE) in fusion reactor plasmas represents one of the greatest potential threats for plasma-facing components [1]. RE in tokamak plasmas usually appear during start-up or shut-down operation phases but, particularly, during the suppression of disruption by massive gas injection (MGI) [2,3]. Injecting a considerable amount of heavy noble gas atoms like Ar, Ne, etc. cools down the boundary plasma, yet this causes RE acceleration and avalanches.
In the case of multi-component plasmas, it has been recognized that energetic electrons could penetrate through the electronic shell of partly ionized heavy ions thus experiencing a non-Coulomb scattering with the bound electrons as well as a Coulomb scattering with the atomic core. Investigations on supra-thermal (non-relativistic) electrons in multi-component plasmas have shown that non-Coulomb collisions contribute significantly to the plasma resistance and affect other transport coefficients [4,5]. The pitch-angle scattering of supra-thermal ions by partly ionized impurities has been considered in [6]. Here, it is shown that non-Coulomb-like scattering also takes place for highly energetic relativistic electrons in multi-component tokamak plasmas. This effect provides a rationale for the hindrance of further RE generation in tokamak plasmas during the mitigation of thermal disruption by MGI.

2. Non-Coulomb collision of RE

As shown in Refs.[1,6], non-Coulomb scattering implies an increase of the cross section for the electron-ion collision. The problem was treated as that of a Coulomb plasma collision with an effective $Z_I(\varepsilon_{kin})$ (where ε_{kin} is the kinetic energy of the incident electrons), which in general is larger than that of the actual Z_I. At low energies, $Z_I(\varepsilon_{kin})$ is equal to Z_I, but at energies of the order of mega-electron-volts, the range of interest here, $Z_I(\varepsilon_{kin})$ may reach the charge of the bare nucleus ξ_I. In the following, it is shown that the model developed in Ref. [4] for the cross section of supra-thermal electron collisions with partially ionized atoms can be generalized to the scattering of highly relativistic electrons within the multi-component plasma and used to find an expression for $Z_I(\varepsilon_{kin})$ over the entire energy range of ε_{kin}. Namely,

$$Z_I^2(\varepsilon) = \xi_I^2 \cdot A_I^2\left[1 + \frac{(1-A_I^2)}{4A_I^2\lambda_I}\ln\left(1+\frac{\varepsilon^2}{\beta_I^2 T_e^2}\right)\right] \quad (1)$$

where $A \equiv Z_I/\xi_I$, is the degree of ionization, ξ_I is the nuclear charge, Z_I is the net, or "shielded" charge of the impurity ion, $\lambda_I = \lambda_i - \ln(Z_I)$ is the Coulomb logarithm for collisions of electrons with impurity ions in the charge state Z_I, λ_i is the Coulomb logarithm for collisions of electrons with background ions, ε is ε_{kin} normalized on electron temperature, T_e and the parameter β is:

$$\beta_I = \frac{6}{T_{e[eV]}} \cdot \left(\frac{\sqrt{\xi_I}}{1-A} \right)^{4/3} \qquad (2)$$

For a bare nucleus, $A=1$ and $Z_I(\varepsilon)=\xi_I$, whereas for a neutral atom, $A=0$ ($\varepsilon \to 0$). Hence, the effective scattering depends only on two parameters, A and ε. Our aim here is to calculate the effective charge value,

$$Z_{eff}(\varepsilon) = \sum_I n_I Z_I^2(\varepsilon) \cdot \lambda_I / \lambda_i \cdot n_e \qquad (3)$$

which represents the ion charge in the case of a multi-component plasma. Substituting $Z_I(\square)$ from (1), one can write the energy dependent effective charge as:

$$Z_{eff}(\varepsilon) = \sum_I Z_I^2 \frac{\lambda_I}{\lambda} \cdot \frac{n_i}{n_e} \cdot \left[1 + \frac{(\xi_I^2 - Z_I^2)}{4 Z_I^2 \lambda_I} \ln\left(1 + \frac{\varepsilon^2}{\beta_I^2 T_e^2} \right) \right] \qquad (4)$$

If we assume for simplicity that only one ion species contributes to the energy dependent $Z_{eff}(\varepsilon)$, while the other ions are fully ionized, we find the following expression for $Z_{eff}(\varepsilon)$:

$$Z_{eff}(\varepsilon) = Z_{eff}(0) \cdot \left[1 + \alpha_I \ln\left(1 + \frac{\varepsilon^2}{\beta_I^2 T_e^2} \right) \right] \qquad (5)$$

where

$$\alpha_I = \frac{(\xi_I^2 - Z_I^2)}{4 Z_{eff}(0) \lambda} \frac{n_I}{n_e} \qquad (6)$$

Here n_I and Z_I are the most representative impurity ion density and charge state for a given temperature T_e [7]. At high energies, $Z_{eff}(\varepsilon)$ can exceed both the charge of impurity ions in the plasma, Z_I, and the nuclear charges of these ions, ξ_I. Indeed, for a plasma with a single ion species, with $Z_{eff}(\varepsilon) \sim \xi_I$, we have $Z_{eff}(\varepsilon) \sim (\xi_I)^2/Z_I \geq \xi_I$ [5]. The representative argon charge state Z_I as a function of temperature is taken from [8] and plotted on Fig. 1 together with the presently calculated $\alpha_I(T_e)$ and $\beta_I(T)$ for the case of Ar impurities (ξ_I=40, λ=15). One can see that he parameters α_I and β drop with increasing plasma temperature for impure plasmas when $n_e Z_{eff} \sim n_I Z_I^2$. Moreover, α_I becomes independent on impurity concentration $\alpha_I(T_e) \sim (\xi_I/Z_I(T_e))^2 - 1$..

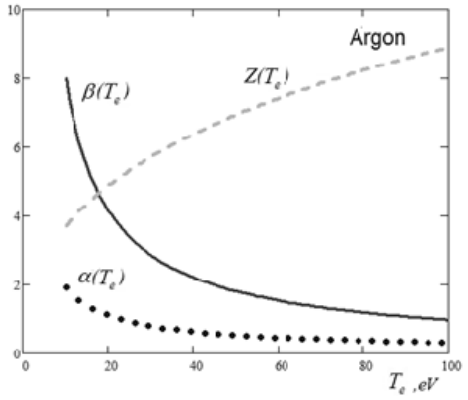

Fig. 1 Dependence of the α, β parameters and the charge state Z_I on the electron temperature for Ar plasma.

The dependence of $Z_{\text{eff}}(\varepsilon)$ on the RE energy was calculated for different electron temperatures. The Argon impurity concentration and the representative charge state are determined from coronal equilibrium [7]. As shown in Fig.2, we find that the increase of $Z_{\text{eff}}(\varepsilon)$ due to non-Coulomb collisions is more pronounce at low temperatures when the impurity ions are slightly ionized. In this case, the difference between the nuclear charge and ion charge is large.

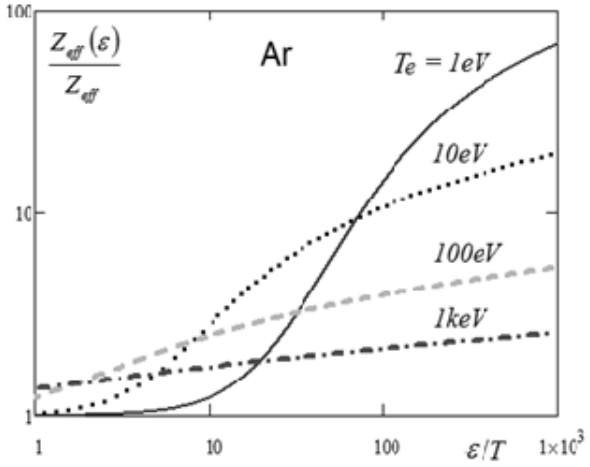

Fig. 2. $Z_{\text{eff}}(\varepsilon)$ (normalized to $Z_{\text{eff}}(\varepsilon=0)$) as a function of RE energy (normalized to the electron temperature) for different plasma temperatures. The Argon impurity concentration and the representative charge state are determined from coronal equilibrium [7].

The penetration of supra-thermal electrons (non-relativistic) into the electron shells of the partially ionized impurities may reduce the plasma transport coefficients (e.g. electron electric conductivity) [4,5]. This, in principle, could cause an unfavorable increase of the required Rosenbluth's suppression density. However, in the cases that we are considering, the number of RE is usually several orders of magnitude smaller than the concentration of thermal electrons in the dense plasma and, therefore, the transport coefficients are determined mainly by thermal electrons. In ITER one expects the average kinetic energy of RE to be E = 12.5 MeV [5], therefore, the relativistic scaling factor, $\gamma = (1-\beta^2)^{-1/2} = E/mc^2$, is ~24 and $\beta \sim 0.99916$, where the average velocity of the RE is βc and m is the rest mass of the electron. By assuming that the plasma current is carried mainly by RE, I_{RE}~10MA, the density of RE can be estimated as $n_{\text{RE}} = I_{\text{RE}}/ec\beta \cdot S \sim 10^{16}\text{m}^{-3}$, which is almost 3-4 orders of magnitude smaller than the thermal density. This indicates that RE will not affect the thermal conductivity and the value of the "Rosenbluth density" will remain unchanged. However, as it will be shown below, the production rate of RE electrons is strongly affected by non-Coulomb collisions of RE.

3. Reduction of runaway production in the case of a non-Coulomb collision

The main population of RE in fusion plasma arises due to multiplication of energetic electrons by close Coulomb collisions with plasma electrons when the electric field exceeds some critical value $E \geq E_{\text{crit}}$. The growth rate of secondary RE can be written as [1]:

$$\gamma_{\text{sec}}(\varepsilon) \equiv -\frac{1}{n_{re}^{I}}\frac{\partial n_{re}^{II}}{\partial t} = \gamma_0 \cdot \sqrt{\frac{\pi \cdot \phi}{Z_{eff}(\varepsilon)+5}} \cdot (\eta - 1) F(\eta, \varepsilon)$$

$$\gamma_0 = eE_{crit} / m_e c \ln\Lambda \qquad (7)$$

where Z_{eff} must be replaced by $Z_{eff}(e)$ (Eq.(5)) in order to take into account the non-Coulomb character of RE scattering $\eta \equiv E/E_{crit}$ and $E_{crit} = 4\pi e^3 \ln\Lambda n_e^* / mc^2$ Here , n_e^* is the electron density of bound and free electrons, and [3]:

$$F(\eta,\varepsilon) = \left\{ 1 - 1/\eta + 6(Z_{eff}(\varepsilon)-1)^2 / \left(\eta^2 + 7.2\right)\left(Z_{eff}(\varepsilon)+5\right)\right\}^{-1/2}$$

The dependence of RE production rate (7) on ε for an electric field that is five times the critical one, $E=5E_{crit}$, is shown in Fig. 3. It demonstrates that the RE grows rate drops considerably because of non-Coulomb collision, particularly for high Z_{eff}.

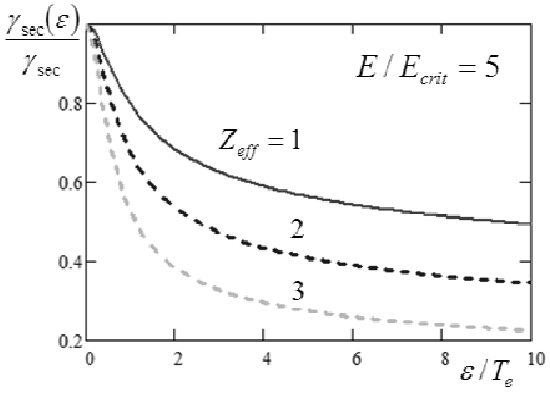

Fig. 3 The growth rate of secondary RE (normalized to $\gamma_{sec}=\gamma(\varepsilon=0)$) vs. RE electron energy (normalized to T_e) for various charge state values (Z_{eff}=1,2 and 3) for $E=5E_{crit}$.

The growth rate dependence on the electric field for a plasma with Ar impurities in different ionization charge states and corresponding to ITER size machine with aspect ratio R/a=3 was calculated (Fig. 4). We again confirm that there is a significant decrease of the growth rate as a result of non-Coulomb collisions of RE.

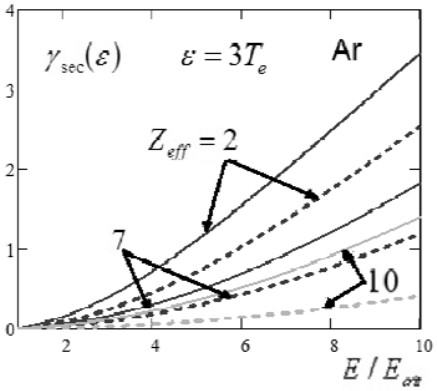

Fig. 4 The growth rate of secondary RE (in γ_0 units) vs. the electric field (normalized to E_{crit}) for different values of effective charge states (Z_{eff}=2,7 and 10).The calculation corresponds to ITER dimensions, R/a=3; dashed lines correspond to cases in which $\gamma_{sec} = \gamma_{sec}(\varepsilon=0)$.

One can also expect an exponential decrease of the primary production of RE with increasing electron kinetic energy. Specifically, the main contribution to the growth rate of primary RE depends exponentially on Z_{eff}. Again, by replacing Z_{eff} by $Z_{eff}(\varepsilon)$ one can write,

$$\gamma(\varepsilon) \equiv -\frac{\partial \ln n_e}{\partial t} \propto \left(\frac{E_D}{E}\right)^{3(1+Z_{eff}(\varepsilon))/16} \cdot \exp\left\{-\sqrt{(Z_{eff}(\varepsilon)-1)\frac{E_D}{E}}\right\} \qquad (8)$$

Although the dependence of $Z_{eff}(\varepsilon)$ is weak (logarithmic) (see Eq.5), the growth rate (Eq.(8)) strongly decreases with increasing ε. Here E is the electric field and $E_D = 4\pi e^3 \lambda_i / T$. The dependence of the production rate (normalized to $\gamma(\varepsilon=0)$.) of primary RE on energy of incident electrons (normalized toT_e), is shown in Fig. 5.

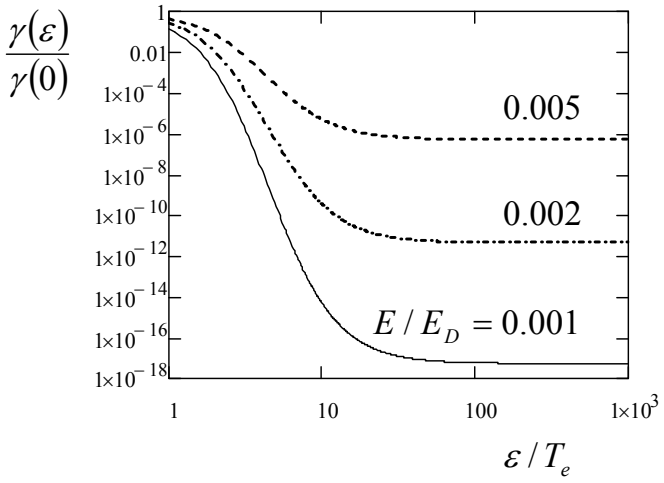

Fig. 5 The growth rate of primary RE (normalized to $\gamma(\varepsilon=0)$) versus the electron energy (normalized to T_e) for different values of the electric field E / E_D.

Conclusion

The penetration of relativistic and supra-thermal electrons through the electronic shells of partly ionized impurity atoms changes the character of their scattering in multi-component plasma from Coulomb to non-Coulomb. These conditions can occur during MGI of heavy atoms at the edge of ITER for the purpose of disruption mitigation. It is found that the deviation from Coulomb cross section reduces the growth rate of primary and secondary RE. Moreover, this reduction is enhanced for increasing RE energy. Non-Coulomb collisions are crucial for slightly ionized impurities when the difference between the nuclei charge and the ion charge state is large. These conditions one can expect during MGI. The growth rate of primary RE decays exponentially due to the dependence of Z_{eff} on the electron energy, whereas that of secondary RE decays according to a power law. Overall these effect could reduce the RE production during MGI in ITER and fusion reactor plasmas and thus must be taken into account in numerical simulations.

References

[1] M. Rosenbluth, S. Putvinski, Nuclear Fusion, Vol. 37, No. 10 (1997)
[2] S. Bozhenkov Analysis of disruptions and their mitigation using ultra-fast observation systems, Berichte des Forschungszentrums Jülich 4288;
[3] S. Putvinski, L. Zakharov, A. Kukushkin, Runaway electron suppression by repetitive gas injection,ITER_D_335UCW, May 2010
[4] V. Kirillov, et al, Sov.J.Plasma Physics.,vol.1(2), p.117,1975
[5] P. Yushmanov.,Sov. J. Plasma Physics.,vol. 6(2), p.259, 1980
[6] P.L. Andrews, R. Goldstone, Princeton University PPPL -1513, 1979
[7] D. Post, R. Jensen, C. Tarter., et al., Nuclear Fusion 17, 1187 (1977).
[8] V. Izzo., Nucl. Fusion 46 (2006) 541–547

Resume

Our activity was mainly devouted to the preparation of issues, needed for DEMO design. Since the design of the rector FW blanket for DEMO is still under disccusion, we have in our calculations considered the most promising nowdays models, namely, a sandwich type made from W alloy as a armor and EUROFER steel as a structural material. It was shown, that

1) Under steady-state operation minimum W armor thickness is limited by the maximum allowable temperature of EUROFER (~550 ºC). The W armor thickness $\Delta_w \sim 3$mm and the EUROFER width $\Delta_{EUROFER} \sim 4$mm are found optimal. The W surface temperature for Δ_w~3mm remains below the melting point and the EUROFER temperature ≤ 550 °C. For the reference case ($\Delta_w \sim 3$mm, $\Delta_{EUROFER} \sim 4$mm) the maximum tolerable heat flux (which does not cause thermal destructions in structural material) is about ~13.5 MW/m^2.

2) To achieve efficient heat transfer required for helium cooling of the FW blanket module in DEMO, a high flow velocity ($\geq$ 100m/s) should be achieved by increasing the pressure drop (~ up to 200MPa inlet pressure). This, unfortunately, could require large pumping power.

3) Direct conversion of the RE magnetic energy into heat within a metallic armor occures du to ohmic dissipation of the return current of free electrons and depends on W surface temperature and RE pulse duration.

4) In the case of hot VDE the W armor is not tolerate the heat load: it melts down to 0.07mm and intensively evaporates up to a few mm during 0.5sec.The RE fast loss case does not cause the W armor melting because of a very short exposure time ~0.01ms. For slow losses the RE deposit their energy (magnetic and kinetic) deeper in armor layer, which explains the W temperature decrease with increasing the armor thickness.

5) Estimation of erosion of the FW by charge-exchange neutrals and the divertor plates by incoming ions shows the importance of angular dependence of sputtering yield and, particularly, the sheath potential effect. We have shown that the sputtering yield increases if the sheath potential is taken into account and that the usual estimation of the sputtering yields at energy $E=3.5ZT_e$ (to account for the sheath effect) underestimates the result.

6) It is found important to account for the angular distribution of incident light ions at low and high temperatures in order to calculate correctly the sputtering yield averaged over the distribution function of the incident particles. Calculations show that under envisaged in DEMO conditions the total sputtering erosion of the FW W armor by the charge-exchange DT neutrals and 5% Helium could reach ~ 1mm during one year of steady-state operation (for particle flux of 10^{19} cm^2/s and T > 100eV). Sputtering erosion from the divertor plates is about 10 times high (without redisposition effect).

7) Our results indicate that high pressure for Helium coolant in inlet is needed to achieve the required heat transfer to the coolant. This requires a big pumping power which could reduce the efficiency of the power conversions. In spite of this deficiency, helium adaptability to any operational temperature makes it very suitable for application in DEMO.

Appendix I

Analysis of a singl noul x-point configuration with respect to coupling of ballooning instability with thermal (MARFE) instability under DEMO conditions
(WP12-PEX-02-T03-01/KIT/PS)

Here we analyse a conventional divertor magnetic configuration (singl nule configuration) with respect to coupling of ballooning instability with thermal (MARFE type) instability [1]. We also consider ballooning instability in the vicinity to x-point. The separatrix and x-point regions are immediate affected by boundary plasma and as a result could trigger MHD instability. However, the feature of MHD perturbation near the x-point is not known. Ballooning modes appear to be the most unstable in this region due to increase of potential magnetic well. The MHD stability can be evaluated by means of ballooning equation for the marginal stability:

$$\left(\vec{B}\nabla\right)\left[\frac{k_\perp^2}{B^2}\left(\vec{B}\nabla\right)\xi\right]+2(1-\gamma)\left(\left[\vec{B}\times\vec{k}_\perp\right]\nabla p\right)\left(\frac{\left[\vec{B}\times\vec{k}_\perp\right]\vec{k}}{B^4}\right)\xi=0 \qquad (1)$$

Metrics of magnetic topology near the x-point can be approximate by topology of the straight current strings combine with the toroidal angle ϕ (see **Fig.1**).

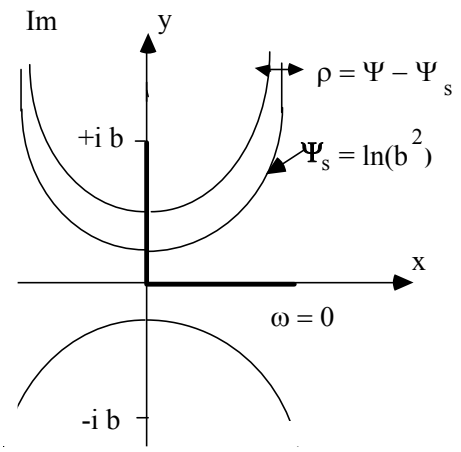

Fig. 1 Magnetic topology of the straight current strings

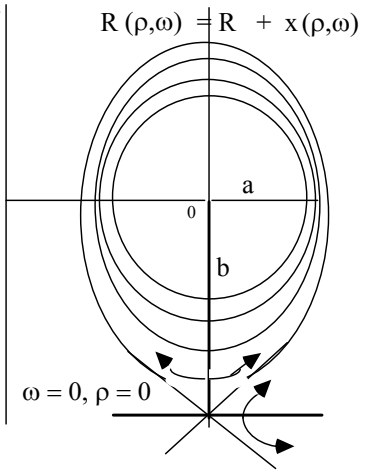

Fig. 2 The magnetic topology of single nule configuration used for ballooning stability analysis.

$$ds^2 = h_\rho^2 d\rho^2 + h_\omega^2 d\omega^2 + R^2 d\phi^2$$

And near the SF region, were ρ,ω <<1

$$h \equiv h_\rho = h_\omega = \frac{b}{2\sqrt{1-\cos\omega+\rho^2/2}}$$

The flux expantion at the SF-region:

$$\Delta_{X-po\,\mathrm{int}} \approx \sqrt{\Delta_{mid-pl.} b}$$

Criterion of ballooning stability near the separatrix can be estimated by using the magnetic topology shown in Fig: 2 the criterion for ballooning stability can be written as [2]:

$$\left.\frac{dP}{d\rho}\right|_{X-po\,\mathrm{int}} < Const.\frac{B^2 R}{q^2}\ \frac{b}{\sqrt{\rho}}, \tag{2}$$

or as:

$$\frac{4\pi q_\pi^{\,2} R}{B^2}\left(\frac{dP}{dr}\right)\Big|_{mid-plane} > \sqrt{\frac{b}{\Delta}} \quad or \quad \left(\frac{dP}{dr}\right)\Big|_{mid-plane} > \frac{b}{P_0}\left(\frac{B^2}{4\pi q^2 R}\right)^2 \tag{3}$$

Where

$$\alpha \equiv \frac{4\pi q_\pi^{\,2} R}{B^2}\left(\frac{dP}{dr}\right)\Big|_{mid-plane} > \frac{b}{P_0}\left(\frac{B^2}{4\pi q^2 R}\right)$$

Here the safety factor q was taken as: $q_\pi(\rho) \equiv q_\pi(0.1) = q_{95}/3$

Neglecting the dependence on shear and assuming that P_0 is the pedestal pressure, one can find that:

$$\left.\frac{\partial P}{\partial r}\right|_{x-po\,\mathrm{int}} \approx \frac{P}{\sqrt{\Delta_{mid.-pl.} b}} < Const.\frac{B^2}{4\pi R q_s^2} s(q,k,\varepsilon,\delta), \quad where\ \ q_s = q_{95}\frac{\pi}{6}\ln(4\pi/\rho),$$

The difference in magnetic potential well for the single nule case is shown in Fig.3

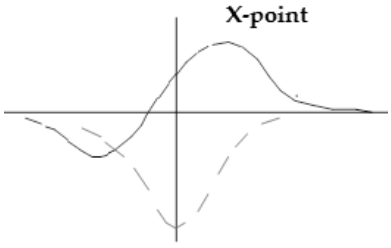

Fig. 3 Magnetic well in the case of a single nule configuration is nonsymmetric: it shifted inwords.

One can conclude that due to different magnetic well inside and outside the critical pressure gradient inside is less than outside. The edge density limitations can be found from ballooning equation.
From Ballooning MHD mode stability ($\Delta_{\text{mid.-plane}} \sim \lambda\ \rho_\theta$) it follows, that the density

$$n_{[10^{20}m^{-3}]} < 1,15\left(\frac{I_{MA}}{\pi a^2}\right)^{3/2}\left(\frac{1}{T_{100}^{3/4}}\right)\left(\frac{R}{a}\right)^{3/4}\frac{A^{1/4}\sqrt{k}}{(1+k^2)^{3/4}}\lambda a\ s(k,\delta,\varepsilon q)$$

From the other side, the requirements to avoid thermal (MARFE) stability

$$\chi_{//}^{0} T^{5/2} / Z_{eff} R^2 q^2 \quad > \quad n^2 C_Z \overline{L_Z}, \qquad \text{where } \overline{L_Z} = (2L - TdL/dT)$$

electron density at the separatrix mid-plane has to be

$$n_{[10^{20} m^{-3}]} = \frac{45 (T_{100})^{7/4}}{qR} \frac{1}{\sqrt{\overline{L_Z} C_Z Zeff}}$$

Thermal - Ballooning stability diagram is shown in Fig. 4.

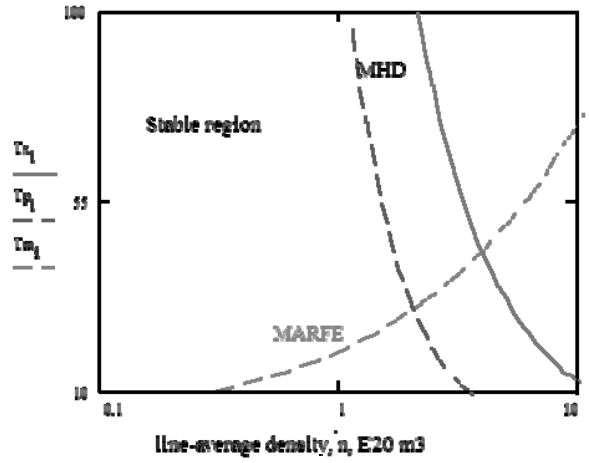

Fig.4 Stability diagram for DEMO. For expecting densities at the edge (>10^{20} m^{-3}) and temperatures above several keV the single nule divertor will be unstable against the coupled ballooning-thermal modes.

Thermal instability (MARFE) is suppressed for higher temperature range, whereas the ballooning modes are unstable for higher pressure. Critical density can for perturbation in inner region (see Fig.6) reads:

$$n_{[10^{20} m^{-3}]} = 1.15 \left(\frac{I}{\pi a_m^2} \right) \frac{a_m^{0.175} R^{-0.3}}{\left(\sqrt{Z_{eff} \alpha \overline{L_{33}} C_Z q_{95}^2} \right)^{3/10}} \left(\frac{A^{1/4} \left(s\sqrt{k\lambda} \right)}{(1+k^2)^{3/4}} \right)^{7/10}$$

and for outer region

$$n_{[10^{20} m^{-3}]} = 0.67 \left(\frac{I}{\pi a_m^2} \right)^{7/9} \frac{1}{\left(Z_{eff} \alpha \overline{L_{33}} C_Z q_{95}^2 \right)^{1/9}} \left(\frac{A (s\lambda)^2}{\sqrt{\frac{R}{a}} (1+k^2)} \right)^{7/18}$$

The analysis of a density limit in tokamaks for DEMO configuration is done for up-down symmetric equilibrium of single nule x-point. The ideal ballooning mode significantly change their feature.

The ballooning perturbation inside the configuration is much weaker, than outside. due to the stabilising effect of a favourable magnetic curvature in inner side. The upper attainable density

exhibits almost linear dependence on the plasma current similar to the Greenwald limit. However it differs from the Greenwald value at low temperatures (<100eV) this limit is less restrictive. A weak dependence on impurity content was obtained. However the influence of impurities can emerge through the resistive modes, which in turn can trigger the ideal modes.

REFERENCES

[1] H. Zohm: On the minimum size of DEMO, Fusion Science and Technology 58
[2] O. Pogutse et al., EPS, 1995

Appendix II

Effect of perpendicular energy transport on the impurity radiation in the SOL and divertor region

The effect of perpendicular energy transport in the low temperature divertor region on impurity radiation loss from the SOL plasma plays an important role [1]. The perpendicular energy transport results in enlargement of the volume with relatively low temperature and a very high density of the plasma. High plasma density causes a strong energy loss due to impurity radiation peak in this low temperature region. For low Z impurity the energy transport due to plasma convection and neutrals also can strongly influence the volume of low temperature region.
The impurity radiation loss is proportional to the electron density, n, the impurity fraction , the local emissivity, L, and the volume of the radiative region, *dV*:

$$W = \int f_Z n^2 L(T,n) dV \approx \overline{f_Z n^2 L \cdot V}_{rad} \qquad (1)$$

The radiative volume V_{rad} is determined by the peak of either f_z , L , or n^2 . Each of those parameters can strongly affect the magnitude of impurity radiation. Experimental observations show that for some cases (MARFE [2], and radiative divertor [2]) a significant amount of radiation (approximately a half) is coming from relatively small volume of rather cold plasma. It is possible that this effect may be explained by the local increase of the emissivity and impurity fraction f_z. However, in this paper we show that even for f_z = const., and L = const. these features of the MARFE and radiative divertor can be explained by high value of n^2V in the low temperature region caused by the perpendicular plasma energy transport.
To estimate impurity radiation loss a simple model based on the balance of the impurity radiation loss and by the energy flux $q = -\chi_e \frac{\partial T}{\partial s}$ transported by the parallel heat conduction χ_e along the magnetic field line, *s* is used.

$$\frac{\partial}{\partial s}(q) = -f_z n^2 L \qquad (2)$$

Multiply Eq. 2 by q and change integration from space coordinate s to the temperature (according the relation $q\partial s = -\chi_e \partial T$) one gets the estimate for impurity radiation:

$$q_\infty{}^2(T_{up}) = q^2(T_{pl}) + \cdot 2\chi_0 \int_{T_{pl}}^{T} f_z \cdot n^2 \cdot L(T) \cdot dT \approx 2\chi_0 \int_{T_{pl}}^{T} f_z \cdot n^2 \cdot L(T) \cdot dT \qquad (3)$$

The radiation loss can be estimated as $W = 4\pi R \cdot \Delta_{sol} \cdot q_\infty$ and assuming that
L = ***L(T).*** and f_z *(T)* from Eq. (1) we arrive to the expression for the maximum poloidal heat flux which can be re-radiated in the region with the temperatures below T (see for example [4])

$$W = 4\pi R \cdot \Delta_{sol} \cdot \sqrt{2\chi_0 \int^{T} f_z \cdot n^2 \cdot L \cdot T^{5/2} dT} \qquad (4)$$

Here $\chi = \chi_0 T^{3/2}$ is the electron conductivity along B. It is small in low plasma temperature region. Therefore, the main contribution to the expression (4) is given by high temperature region of the SOL plasma It is true even for the low Z impurities like carbon [4] and coronal approximation for L(T) , which is strongly peaked at low temperatures. The reason for this is a small volume of the low temperature plasma caused by the strong temperature gradient due to small χ. But, this conclusion means that the radiation loss for the low Z impurity from the plasma core should be much higher due to larger volume and higher plasma density. However, we show here that the perpendicular plasma transport is very important for the estimates olof the factor $n^2 V_{rad}$ in low temperature region. Actually, one can see it just from Eq. (2). The width Δ_{sol} should be found self consistently from the energy balance equation because of the competition of parallel and perpendicular plasma transport. In the simplest case, when the electron heat conduction is dominant we have

$$\nabla_\perp(-\chi_\perp \nabla_\perp T) + \frac{\partial}{\partial s}\left(-\chi \frac{\partial T}{\partial s}\right) = f_z n^2 L \qquad (5)$$

From Eq. (5) we may conclude that $\Delta_{sol} \approx \sqrt{\chi / \chi_\perp}$ Substituting this estimate in Eq. (4) we find

$$W \approx \sqrt{\chi / \chi_\perp} \cdot (..\chi.)^{1/2} \propto \sqrt{\chi_\perp} \qquad (6)$$

and W does not depend on the magnitude of χ. To treat Eq. (5) more accurately let divide the SOL plasma in two regions: a) the high temperature SOL mantle, and b) the low temperature divertor region. In the region of the high temperature SOL mantle we can only retain in Eq. (3) the radial (r) derivative in the term $\nabla_\perp(\chi_\perp \nabla_\perp T)$.

In the attached case, when electron pressure remains const. along the magnetic field lines, $p=n_e T_e$ Eq. 4 can be written as

$$W = 4\pi R \cdot \Delta_{sol} \cdot p \sqrt{2\chi_0 \int^T f_z \cdot L \cdot T^{1/2} dT} \qquad (7)$$

and the r.h.side in Eq.(7) becomes purely temperature dependent.

Radiation from the upstream SOL high temperature region (mantle) can be estimated from Eq. 5 by retaining only radial derivatives and consider the parallel heat transport to the divertor region as a sink:

$$\frac{\partial}{\partial r}(-\chi_\perp \frac{\partial}{\partial r} T) = f_z n^2 L + \frac{\partial}{\partial s}\left(\chi \frac{\partial T}{\partial s}\right) \approx f_z n^2 L + \chi_0 \frac{T^{7/2}}{l_{sol}^2} \equiv R_{imp}(T) + E_{div}(T) \qquad (7)$$

From Eq. (5) we find the radiation loss in the SOL mantle, W_{SOL} , and the energy flux coming into divertor, Q_{div}:

$$W_{sol} = \frac{S_{sol} \cdot \int^{Tsep} \chi_\perp R_{imp}(T) dT}{\sqrt{2\chi_0 \int^T \chi_\perp (R_{imp}(T') + E_{div}(T')) dT'}} \qquad (8)$$

$$Q_{div} = \frac{S_{sol} \cdot \int_{}^{Tsep} \chi_{\perp} E_{div}(T) dT}{\sqrt{2\chi_0 \int_{}^{T} \chi_{\perp} (R_{imp}(T') + E_{div}(T')) dT'}} \tag{9}$$

where S_{sol}, is the tokamak surface at the separatrix, and the separatrix temperature, T_{sep}, is determined by the energy flux, Qs, coming into the SOL from the bulk plasma

$$Q_s = \sqrt{2 \int_{}^{Tsep} \chi_{\perp} \cdot (R_{imp}(T') + E_{div}(T')) dT} \tag{10}$$

Let us estimate the fraction of the radiation loss from the SOL mantle, $\delta_{sol} = W_{sol}/Q_s$, for the model function of the impurity radiation $R_{imp}(T) = f_z n^2 L(T) = const. = R$, and $\chi_{\perp} \sim$ const, $E_{div} \sim T^{7/2}$ Then

$$\delta_{sol} = \frac{1 \int_{}^{Tsep} \chi_{\perp} E_{div}(T) dT}{2\sqrt{2\chi_{\perp} \int_{}^{T} (R_{imp} + E_{div}(T')) dT'}} \approx 0.5 \cdot \frac{\int_{0}^{\theta} \frac{1}{\sqrt{y^{9/2} + y}} dy}{\theta^{9/2} + \theta} \tag{11}$$

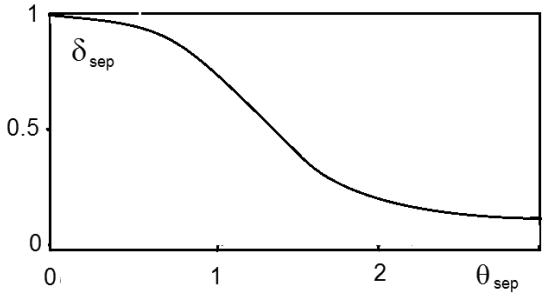

Fig. 1 Radiation flux from the SOL mantel vs. the separatrix temperature

where $\theta_{sep} = T_{sep}/T^*$ and $E_{div}(T^*) \equiv R$. From Fig. 1 one can see that $\delta_{sol} = W_{sol}/Q_s \sim 1$ for $\theta_{sep} < 1$ and it decreases rapidly with increasing θ_{sep}, for $\theta_{sep} \leq 1$. The case $\theta_{sep} < 1$, when there is practically a complete re-radiation of the energy flux incoming into the SOL requires a very careful analysis of the radiation losses in the core plasma, since the energy balance can be fragile. Below we will assume that $\theta_{sep} \geq 1$ and the radiation loss from the SOL mantle is small.

Radiation loss from the divertor volume can be evaluated from Eq.5 in slab geometry.

$$\frac{\partial}{\partial y}((\chi_{\perp} + b^2 \chi)\frac{\partial T}{\partial y}) + \frac{\partial}{\partial \rho}(\chi_{\perp}\frac{\partial T}{\partial \rho}) = R \tag{12}$$

where y and ρ are the poloidal and radial coordinates, and b is the ratio of the poloidal and the total magnetic field strengths $b = B_{pol}/B_{tor}$,. Introducing the vector **n** (see Fig. 2) and neglecting the

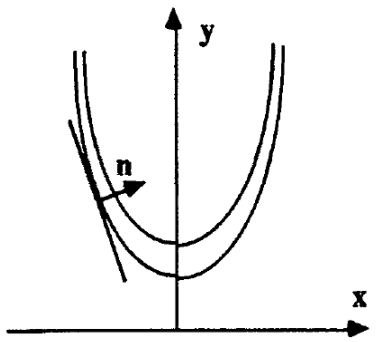

Fig. 2 Temperature contours in a divertor

curvature of the temperature contours we can represent Eq. (12) in the form

$$\frac{\partial}{\partial l_n}((\chi_\perp + (\mathrm{n}\cdot y)^2 b^2 \chi)\frac{\partial T}{\partial l_n}) = R \tag{13}$$

where l_n, is the coordinate along **n**. As we mentioned above, the estimate of the factor $(n_e)^2 V_{rad}$ in a low temperature region based on the parallel heat conduction (see Eq.(2)) results in the radiation loss from the SOL mantle, which we assume to be small. Therefore, we can negiect the term with χ in Eq. (13). Then, from Eq. (13) we find the estimate for the impurity radiation loss from the low temperature divertor region, Q_{div}, caused by the perpendicular heat transport

$$Q_{div} = S_{rad\,front} \cdot \sqrt{2\int^{\infty} \chi_\perp(T) R_{imp}(T) dT} \tag{14}$$

where $S_{rad\,front}$, is the surface of the radiating flame front. For the upper limit of the integral in Eq. (14) we choose infinity, but practically it does not matter. Indeed, assuming that the plasma pressure is constant along the magnetic field lines and f_z= const. we find $R=f_z p^2 L(T)/T^2$ and

$$\chi_\perp = \kappa_\perp \cdot n = p \cdot \kappa_\perp / T$$

In this approximation, the integral in Eq. (14) converges unless κ perp, f_z or L increases very rapidly with increasing temperature. Therefore, perpendicular plasma heat transport causes a strong impurity radiation loss in the low temperature region.

Above we have assumed that only plasma heat conduction causes the energy transport. However, low Z impurities like carbon can have a peak of radiation loss in the temperature range below 10 eV. For this relatively low temperature region the effects of the plasma conduction and neutrals on the energy transport can be important. 2D transport model shows that almost 100% of Carbon radiation is coming from a low temperature (≤10 eV) divertor region. In the radiative region a significant fraction of the energy is transported by plasma convection and neutral energy transport.

Integration of Eq. 13gives impurity radiation loss from divertor Qrad, div (see radiation loss estimate for main chamber):

$$q_\perp = S_{rad,flame} \cdot 2 \int_0^{T_C} n_e^2 f_Z L_Z(T_e) \kappa_\perp \, dT_e \, ,$$

but now the surface of the radiating front ($S_{\text{rad flame}}$) enters, which is, because of perpendicular transport, much larger than for the case without (see **Fig.3**).

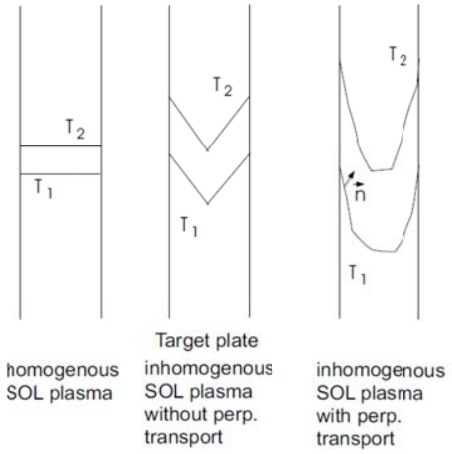

Fig. 3 Plasma temperature contours in the divertor for a homogeneous SOL plasma (left), an inhomogeneous SOL plasma without perpendicular transport (middle) and an inhomogeneous SOL plasma with perpendicular transport (right). The surface of the radiating front increases strongly from the left to the right and by this one gets much larger radiation losses [1] .

In conclusion one can state that

1) the perpendicular energy transport results in a strong enlargement of the plasma volume with relatively low temperature and very high density. High plasma density causes a strong energy loss due to impurity radiation peak in this low temperature region.
2) Analytical estimates, accounting the perpendicular energy transport, show that the impurity radiation loss from the low temperature region like MARFE and radiative divertor increases drastically and can be dominant.
3) the energy transport from cold divertor region is significantly affected by the plasma convection and the neutral energy transport.

References

[1] S.I. Krasheninnikov and D.A. Knoll. Effect of perpendicular transport on edge plasma energy loss due to impurity radiation. *Contributions to Plasma Physics*, 36(2.3):266.270, 1996. 5th Workshop on Plasma Edge Theory, December 1995, Asilomar, USA.
[2] Lipshultz B., J. Nucl. Mater. 1458~147, (1987) 15.
[3] Porter G., Bulletin of the American Physical Society, 40 (1995) 1693.
[4] Post D. E., J. Nucl. Mater. 220&222,

Appendix III

Sputtering yield for the PF components under reactor plasma edge conditions.

Here the updated version of the work published erlier in Journal of Nuclear Materials 162-164 (1989) 462-466 (by V. Abramov, Yu. Igitkhanov, et al., Wall and Divertor Plate sputtering in tokamak reactor) is presented. In this work the sputtering yields averaged over energy and angular distributions of incident deuterium and tritium ions on various materials proposed for the divertor plates and first wall of a tokamak reactor (C, Al, Ti, Fe, MO, W) is calculated. Modifications to the particle distribution function due to acceleration in the sheath electric field are included and the calculations are performed over the energy range characteristic of the particles in the plasma boundary. The results are restricted to the case of magnetic field lines normal to the divertor plate surface.

Calculations of the sputtering yield for first wall materials have been performed in several papers (see, e.g. ref. [30]), Assuming normal incidence, the different expressions are extrapolated to the low energy range characteristic of the plasma edge and used to calculate the divertor plate erosion rate. In general, the sputtering yields so obtained correspond to those which would be produced by particles whose are consistent with acceleration through the Debye sheath. It is easy to show that the thickness, A of structural elements sputtered during one year of continuous operation, by particle fluxes of different species j, can be expressed as

$$\Delta = \frac{5.27 \cdot 10^{-16}}{\rho} A \sum_j \left\langle S_j q_j \right\rangle \qquad (1)$$

Here Δ is in mm/year, A is the target atom mass (in amu), ρ is the target material density (g/cm3), $S_j(E,\theta)$ is the sputtering yield of particle j with energy E and angle of incidence θ and q_j, is the flux of particles j (particles cm^{-2} s^{-1}). The brackets $\langle\ \rangle$ represent an average over the angular and energy distribution of incident particles. Thus, the precise determination of the erosion rate needs the correct form of the energy distribution function of the incident particles and the sputtering yield $S_j(E,\theta)$. Although a Maxwellian distribution is commonly chosen, the distribution function of charged particles near the divertor plates may be strongly distorted. This paper presents the results of erosion rate calculations taking into account modifications of the distribution function and the angular dependence of the sputtering yield.

1. Distribution function of incident particles

Let us consider the distribution function for particles arriving at a material surface. It is clear that many effects can influence the energy distribution function near the divertor plates. In practise, it is impossible to take into account all of these effects by an exact method. For this reason we consider only the main effects which determine the difference between the near and far distribution functions in the edge plasma flow.

Far from the divertor plates, the ion distribution function can be considered a Maxwellian shifted by some velocity V_0. The longitudinal gradients in the boundary plasma, particle sources and acceleration in the presheath field determine the value of V_0, [31]. For typical boundary plasma parameters the inequality $\rho_e \le \lambda_D < \rho_i < \lambda_p$ is satisfied ($\rho_{e,i}$ is the electron (ion) Larmor radius, λ_D is the Debye length and λ_p - the mean free path of a charged particle). If λ_p, exceeds the characteristic length of the neutral atom distribution near the plate, then this neutral gas will not influence the charged particle distribution function. This condition is satisfied if the plasma density, which determines the width of the neutral atom spatial distribution exceeds or is comparable with

the atom density. The effect on the distribution function of a magnetic field and of ionization of atoms may be neglected for the conditions considered here.

The ion velocity distribution at the plasma sheath interface (i.e. at a distance λ_D, from the plate) can be expressed as

$$f_0(M_0) = \frac{2j_0}{V_T^2}\frac{1}{\pi V_T^2}\exp\left[-u_{\perp 0}^2 - (u_{//0} - M_0)^2\right] \qquad (2)$$

where $j_0 = n\sqrt{T/2\pi m_i}$ is the ion flux to the plate, $u_{\perp 0} = V_\perp / V_T$, $u_{//0} = V_{//} / V_T$ are the transverse and longitudinal components of the velocity along the magnetic field normalized to the thermal velocity $V_T = \sqrt{2T_i / m_i}$ and $M_0 = V_{//} / V_{T0}$. Expression (2) represents the distribution function for collisionless ions accelerated by the presheath field so that at the entrance to the sheath their mean velocity satisfies the Bohm sheath criterion. According to this condition, the value of M_0 at the plasma-sheath interface is given by $M_0 = \sqrt{Z_j e\varphi_0 / T_i} \approx \sqrt{Z_j / 2}$ where Z_j is the charge of an ion accelerated in the presheath field, $e\varphi_0 \sim T_e / 2$.

In so far as that in this regime the distribution function is determined only by the constants of motion, near the plate the distribution function is

$$f = \iint f_0(u_{//0}, u_{\perp 0})\delta\left(u_\perp^2 - u_{\perp 0}^2\right)\delta\left(u_{//}^2 + \frac{Z_j e(\varphi - \varphi_0)}{T_i} - u_{//0}^2\right)du_{//0}^2 du_{\perp 0}^2 \qquad (3)$$

Here φ is the plasma potential far from the plate, and δ is the Dirac delta function. Taking the plate potential to be zero, the distribution function for the ions at the plate may be written as:

$$f_d = \begin{cases} \dfrac{2j_0}{V_T^4 F(M_0)}\exp\left(-u_\perp^2 - \left(\sqrt{u_{//}^2} - \dfrac{Z_j e\varphi_0}{T_i} - M_0\right)^2\right) & u_{//} > \sqrt{\dfrac{Z_j e\varphi_0}{T_i}} \\ f_d = 0 & u_{//} < \sqrt{\dfrac{Z_j e\varphi_0}{T_i}} \end{cases} \quad ,(4)$$

and $F(M_0) \equiv 2\pi\int_0^\infty f(V)dV_\perp \int_0^\infty V_{//}dV_{//} = e^{-M_0^2} + \sqrt{\pi}M_0 Erf(-M_0)$ (5)

It should be noted that in obtaining eq. (4) the ions are assumed to completely recombine on the plate and the lines of force are assumed to be oriented normally to the divertor plates. Clearly, if the angle, θ, between the normal to the plate and the line of force increases, then the value of M_0, which is proportional to $\cos\theta$ tends to zero. In the limiting case of grazing incidence ($\theta \to \pi/2$) the distribution function (4) transforms into an unshifted Maxwellian. The effect of the magnetic field can be neglected in this case since $\rho_i > \lambda_D$. The dependence of the shift in the distribution function on the inclination angle of the line of force is connected with the fact the sheath electric field is oriented normal to the surface. The value of the component of this field along the direction of the lines of force decreases when the inclination angle increases. In reality, they are normal and tangential intersections of the lines of force with the surface because of surface roughness. The most unfavourable case, corresponding to normal incidence (θ = 0), has been taken into account in the calculations of sputtering yields which follow. The usual expression for the potential drop in the sheath is used: $e\varphi_0 \approx T_e \ln\sqrt{m_i / 2\pi m_e}$ .This expression is valid in the absence of secondary electron

emission and if the inequality $\sum_k n_{Z_k} Z_k << n_i$ is satisfied, (n_i is the plasma ion density and n_z, is the density of impurity ions in ionization state Z_k ,). From eq. (4) we note that in general there is a large difference between the distribution of ions arriving at the plate and a simple Maxwellian. For the distribution function of neutrals near the plate, we assume the ion distribution function of eq. (2). This assumption is based on the fast relaxation (over a time of order the collision time) of the distribution function of cold atoms leaving the plate surface to the ion distribution function near the plate. We assume further that the distribution function of the atoms arriving at the first wall is also Maxwellian.

2. Energy dependence of the sputtering yield

We now turn to the energy dependence of the sputtering yield for the case of normal incidence. The exact solution of the sputtering yield problem for the low energy range $E < 1keV$ has not obtained yet. For this reason, we must use empirical relations that agree well with the available (scarce) experimental data. The following expression for the sputtering yield is proposed in [32-34]:

$$S_1(E,0) = \frac{C}{U_0} Z_1^{3/4} (Z_2 - 1.8)^2 \left(\frac{M_1 - 0.8}{M_2} \right)^{3/2} \cdot \frac{(E - E_{TH})}{\left(E - E_{TH} + 50 Z_1^{3/4} Z_2^{3/4} \right)^2} \tag{6}$$

where $C = 2 \cdot 10^3$ for hydrogen atoms (ions) and $C = 400$ for other projectiles. U , is the binding energy of the surface atoms (sublimation energy) in eV , Z_1, Z_2, M_1, M_2 are the atomic numbers and masses (in amu) of the target and projectile respectively, $\boldsymbol{E}$ is the projectile energy (eV) and E_{TH} **,** is the threshold energy given by the expression (7):

$$E_{TH} = \frac{(4M_1 + M_2)^2}{4M_1 M_2} \tag{7}$$

From equation (6) we see that $S_1 \sim 1/E_1$ for large E but the experimental data agree fairly well with the law $S \sim \ln E / E$ [33]. The expression proposed in [34], based on the results of both theoretical and experimental investigations, and predicts just such energy dependence.
According to [34] the sputtering yield is

$$S_2(E,0) = Q \left\{ 3.441 \sqrt{\frac{E}{E_{TF}}} \ln\left(\frac{E}{E_{TF}} + 2.718 \right) \cdot \left[1 - \left(\frac{E}{E_{TF}} \right)^{-2/3} \right] \cdot \left(1 - \frac{E_{TH}}{E} \right)^2 \right\} \cdot F(E, E_{TH}) \tag{8}$$

where

$$F(E, E_{TH}) = \left\{ 1 + 6.355 \sqrt{\frac{E}{E_{TF}}} + \frac{E}{E_{TF}} \left(6.882 \sqrt{\frac{E}{E_{TF}}} - 1.708 \right) \right\}^{-1} \tag{9}$$

Here, E_{TF} **,** is the energy in the centre-of-mass system for a head-on collision with the screening radius for a Thomas-Fermi potential as the closest approach and E_{TH} **,** is the threshold energy. The parameters Q, E_{TF}, E_{TH} are given in [34] for some representative cases. Calculations show that the predictions of equation (8) are somewhat closer to the experimental data than those from equation (6). We therefore choose the former for use in our estimation of the sputtering yields at low energy.

3. Angular dependence of the sputtering yield

Several authors (see, e.g. [32]) have considered the sputtering yield dependence on the projectile angle of incidence.

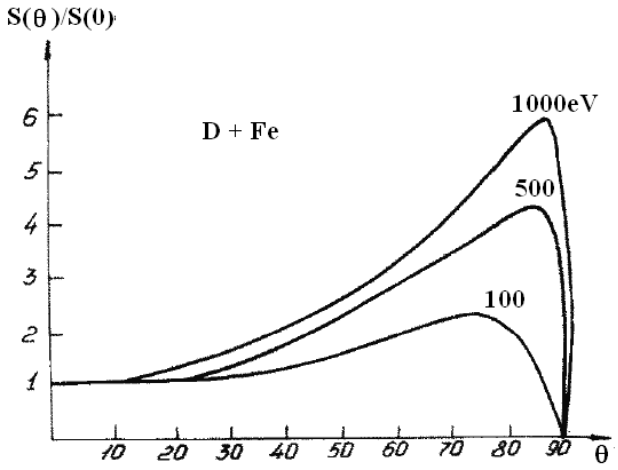

Fig. 1. The angular dependence of the sputtering yield $S(\theta)$ for varying projectile energy.

The most complete treatment is given in [34], according to which the following approximation may be used:

$$S(\theta) = \frac{1}{\cos^{f}\theta} \exp\left\{ - f \cos\theta_{opt} \cdot \left(\frac{1}{\cos\theta} - 1 \right) \right\} \qquad (9)$$

The parameters f and θ_{opt}, have been determined both from available experimental data and numerical calculations. f is independent of projectile energy for the case of sputtering by light ions, and θ_{opt} (in degrees) is given by the expression

$$\theta_{opt} = 90^{\circ} - 57.3 \frac{\eta}{E^{1/4}} \qquad (10)$$

f and η (for $E = 1$ keV) are given in ref. [35] for H, D, T, He and various target materials. **Fig. 1** shows the function $S(\theta)$ for the combination (D +Fe). It should be noted that equation (9) and (10) predict the angular dependence of the sputtering yield well only for light ion sputtering. Their validity to the case of heavy ion sputtering is doubtful, especially if calculations of the sputtering yield averaged over an energy spectrum are required. In addition, it can be shown that the sputtering yield averaged over the energy and angular distributions of the incident particles is very sensitive to the behaviour of its components in the near threshold energy range and near $\theta = 90^{\circ}$. There is evidence that equations (9) and (10) are not valid in this case.

4. The average sputtering yield

The twice-averaged sputtering yield, which we define as the yield averaged over the distributions of energy and angle of incidence of the projectiles, is given by

$$\overline{S_j} = \frac{\int f_d S(E,\theta) V_{//} dV}{\int f_d V_{//} dV} =$$

$$= \frac{\int f_d(E,\theta)) S(E,\theta) \sqrt{E} dE \cos\theta \cdot d(\cos\theta)}{\int f_d(E,\theta)) \sqrt{E} dE \cos\theta \cdot d(\cos\theta)} \qquad (11)$$

This expression may be transformed to the following

$$\overline{S_j}\left(\frac{atom}{ion}\right) = S_{T_0}\int_0^1 tS(t)\int_{\varepsilon^*}^{\infty}\exp\left(-\frac{\varepsilon}{\beta}\left(1-t^2\right)\right)S(\varepsilon)\exp\left[-\left(\sqrt{\frac{\varepsilon}{\beta}t^2-\delta}-M_0\right)^2\right]\varepsilon d\varepsilon \qquad (12)$$

where

$$S_{T_0} = \frac{2E_T^2}{T_i^2 F(M_0)}, \qquad t = \cos\theta, \qquad \varepsilon^* = \max(1,\delta); \qquad \varepsilon = E/E_{TH}$$

$$\beta = T_i/E_{TH} \qquad \delta = Z_j e\varphi_0/T_i$$

In equation (12) $S(t)$ represents, the angular dependence of the sputtering yield [see eq. (9)] and $S(\varepsilon)$ the energy dependence [see eq. (9)]. We note that the dependence of $\overline{S}$ on δ (i.e. on Z_j and φ_0) is rather complex. On the one hand $\overline{S}$ evidently increases when δ increases due to an increase in the population of fast particles, but on the other hand, $\overline{S}$ must decrease if the minimum energy gained in the sheath exceeds the threshold energy so long as the integration region over ε decreases when δ increases.

Results and conclusions

In accordance with the above, we have calculated the twice-averaged sputtering yields for a number of target/projectile combinations. Table 1 shows the results for deuterium ion sputtering. Table 2 shows the results for the same target materials but for the case of incident tritium ions. It is interesting to note that in both cases the sputtering yield decreases as the target mass increases in this low energy range; this is valid even for mono-energetic ions.

Table I

Variation of the twice averaged sputtering yield, $\overline{S}$ for various target materials as a function of the temperature of incident deuterium ions

T (eV)	Target					
	C	Al	Ti	Fe	Mo	W
5	3.23(−3) [a]	2.2(−4)	1.75(−5)	6.8(−5)	2.8(−12)	2.63(−14)
10	1.97(−2)	5.8(−3)	1.08(−3)	2.94(−3)	3.9(−7)	3.62(−8)
50	5.85(−2)	5.1(−2)	1.8(−2)	3.95(−2)	2.6(−3)	1.53(−3)
100	5.63(−2)	6.06(−2)	2.44(−2)	5.36(−2)	6.3(−3)	4.57(−3)
500	2.9(−2)	4.45(−2)	2.32(−2)	5.4(−2)	1.1(−2)	1.07(−2)
1000	1.9(−2)	3.18(−2)	1.8(−2)	4.29(−2)	1.01(−2)	1.11(−2)

[a] Note: 3.23(−3) means 3.23×10^{-3}.

Table 2

Variation of the twice averaged sputtering yield $\bar{S}$, for various target materials as a function of the temperature of incident tritium ions T (ev)

T (eV)	Target					
	C	Al	Ti	Fe	Mo	W
5	1.82(−3) [a]	7.99(−4)	1.6(−4)	3.12(−4)	4.15(−7)	1.62(−12)
10	2.94(−2)	1.24(−2)	3.97(−3)	7.81(−3)	1.6(−4)	3.59(−7)
50	1.94(−1)	7.72(−2)	3.63(−2)	7.37(−2)	1.08(−2)	3.57(−3)
100	2.12(−2)	8.99(−2)	4.68(−2)	9.7(−2)	1.75(−2)	9.29(−3)
500	1.3(−1)	6.52(−2)	4.31(−2)	9.57(−2)	2.36(−2)	2.00(−2)
1000	8.9(−2)	4.66(−2)	3.32(−2)	7.60(−2)	2.08(−2)	2.05(−2)

[a] Note: 1.82(−3) means 1.82×10^{-3}.

These calculations enable us to estimate the relative importance of the effects of acceleration in the sheath potential, modifications of the distribution function and the angular dependence of the sputtering yield. Analysis of the results shows that variations in the sputtering yield are mainly due to the accelerating potential. So, if for example, we take into account only the angular dependence for deuterium atoms at $T = 100eV$ incident on tungsten, then the sputtering yield is increased by about a factor 3 over that for the case of normal incidence. Taking into account the sheath acceleration the yield is enhanced by a factor 35. Fig. 2 show the effect of the angular dependence on the sputtering yield. One can see that the ratio of the twice averaged yield to the energy averaged yield (for the case $\delta = 0$, $M_0 = 0$) increases as the temperature increases. This result is expected so long as the fast particle population increases as the temperature increases since, from equation (9) the yield is enhanced as grazing incidence is approached. The above leads us to the following conclusion: despite the weak dependence of the sputtering yield on the angle of incidence

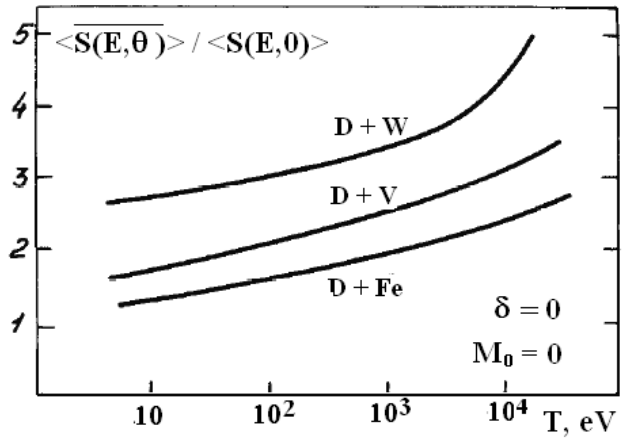

Fig. 2. Ratio of the sputtering yield averaged over energy and angle of incidence to the yield averaged over energy only (i.e. for $\theta = 0$).

in the energy range below 200 eV, it is essential to account for the angular dependence in this range if the energy averaged sputtering yield is to be accurately predicted. For example, even at $T = 10eV$, the enhancement factor is 2.5 for D-W sputtering. The calculated data also show that the distribution function distortion introduced by the sheath acceleration effect leads to sputtering yield increases of 1.5-2. This enhancement is comparable with that due to the angular effect. As an illustration, it is interesting to compare the calculated values of the yield with those obtained from equation (8) for $E = 5.5Z_jT_e$ the energy gain because of acceleration in the sheath and pre-sheath

electric fields. It is easy to show that for all projectile/target combinations the values of s given in tables 1 and 2 exceed those of $S_2(3.5ZT)$ the actual enhancement factor depends on the type of projectiles' result also valid if we use expression (8) to estimate the sputtering yield for $E = 5.5.Z_jT_e$.The sputtering yields averaged over the distribution function and over the projectile incident angle have been obtained for some candidate target materials (C, Al, Ti, Fe, MO, W) and incident deuterium and tritium ions.

We have shown that the sputtering yield increases if the sheath potential is taken into account and that the usual estimation of the sputtering yield at energy $E = 3.5Z_jT_e$ is too low

It is found that it is essential to account for the angular distribution of incident light ions at low and high temperatures in order to calculate correctly the sputtering yield averaged over the distribution function of the incident particles [36]. Duble averaged sputtering yield of W by various elements is shown in **Fig. 3.**

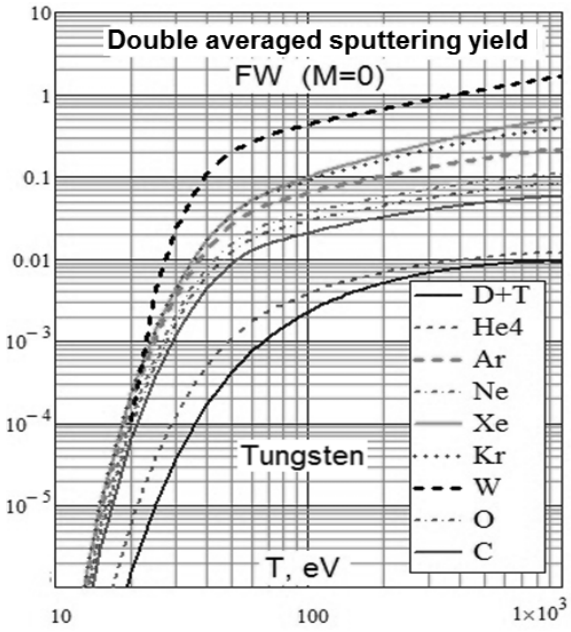

Fig. 3. The sputtering yields of W averaged over energy and angle of incidence taken for various incedent ions are shown; the ions are at the most representative ionization charge state at given temperature [8]

References

[1] Guseva M.,. Ionova E and Martynenko Yu., IAE preprint IAE- 3225 (1979).
[2] Igitkhanov Yu., Pistunovich V.and Pozharov V., IAE preprint IAE-4217/8 (1985).
[3] Smith D.et al. Proc. 9th Symp. on Engineering Problems in Fusion Research, Chicago, IL, USA, 1981.
[4] Martynenko Yu., Itogi nauki i tekniki [Science and Tech. Results] 3 (1982) 119.
[5] Bohdansky J. et al. Nucl. Fusion Special issue (1984) 61.
[6] Yamamura Y., Itikawa Y. and Itoh N., Institute of Plasma Physics, Nagoya University, Report IPPJ-AM-26 (1983).
[7] Igitkhanov J., Journal of Nuclear Materials 162-164 (1989) 462-466
[8] Post D. E., Jensen R. V., Tarter C. B., Grasberger W. H., Lokke W. A., *Atomic Data and Nuclear Data Tables* 20, 397-439 (1977).

ISSN 1869-9669